REVIEW ARTICLE

# APT-Weighted MRI: Techniques, Current Neuro Applications, and Challenging Issues

Jinyuan Zhou, PhD,[1,2*] Hye-Young Heo, PhD,[1,2] Linda Knutsson, PhD,[1,3] Peter C.M. van Zijl, PhD,[1,2] and Shanshan Jiang, MD, PhD[1,2]

Amide proton transfer-weighted (APTw) imaging is a molecular MRI technique that generates image contrast based predominantly on the amide protons in mobile cellular proteins and peptides that are endogenous in tissue. This technique, the most studied type of chemical exchange saturation transfer imaging, has been used successfully for imaging of protein content and pH, the latter being possible due to the strong dependence of the amide proton exchange rate on pH. In this article we briefly review the basic principles and recent technical advances of APTw imaging, which is showing promise clinically, especially for characterizing brain tumors and distinguishing recurrent tumor from treatment effects. Early applications of this approach to stroke, Alzheimer's disease, Parkinson's disease, multiple sclerosis, and traumatic brain injury are also illustrated. Finally, we outline the technical challenges for clinical APT-based imaging and discuss several controversies regarding the origin of APTw imaging signals in vivo.

**Level of Evidence:** 3

**Technical Efficacy Stage:** 3

J. MAGN. RESON. IMAGING 2019;50:347–364.

MAGNETIC RESONANCE IMAGING (MRI), invented and applied to the human more than 40 years ago, is a highly versatile imaging technology used in radiology to image basic anatomy and function with microliter resolution. Currently, MRI is a key modality for diagnosing disease, guiding treatments, and assessing the effects of treatment. A few conventional pulse sequences, such as $T_2$-weighted ($T_2$w), fluid-attenuated inversion recovery (FLAIR), $T_1$-weighted ($T_1$w), and particularly gadolinium-enhanced $T_1$-weighted (Gd-$T_1$w) MRI are the main tools in daily clinical practice. Since the 1990s, several advanced, more tissue function-oriented sequences, such as perfusion imaging, diffusion imaging, and proton MR spectroscopic imaging (MRSI), have been introduced to some clinical research protocols. As MRI is applied further at the molecular level, more possibilities for disease diagnosis and treatment assessment are becoming evident.[1] Currently, however, most molecular MRI studies rely on the administration of paramagnetic or superparamagnetic metal-based substrates that are not biodegradable and will have to go through a lengthy testing and protocol approval before becoming available in the clinic. Ideally, molecular imaging would exploit endogenous molecules that can be probed noninvasively using existing hardware.

Combining nuclear magnetic resonance (NMR) concepts of chemical exchange and signal saturation, as originally proposed by Forsen and Hoffman,[2] Balaban and colleagues first demonstrated that the process of saturation transfer from exchangeable protons to water can be used for enhancing the detection sensitivity of molecules, a molecular imaging approach dubbed chemical exchange saturation transfer (CEST) imaging.[3] Based on this approach, numerous low-concentration endogenous biomolecules or exogenous imaging agents with water-exchangeable chemical groups and tissue physicochemical properties (eg, pH) that influence the exchange rate can be detected indirectly through the bulk water signal used in MRI.[4–9] The most studied type of CEST MRI to date, amide proton transfer (APT) imaging,[10] is geared towards detecting the exchangeable amide protons in the backbone of mobile proteins, previously visualized in the in vivo proton NMR spectrum.[11,12] With this technique, these proteins can be imaged in vivo using the water signal, thus enabling translation to clinical MRI scanners. When using the

View this article online at wileyonlinelibrary.com. DOI: 10.1002/jmri.26645

Received Nov 18, 2018, Accepted for publication Dec 27, 2018.

*Address reprint requests to: J.Z., Division of MR Research, Department of Radiology, Johns Hopkins University School of Medicine, 600 N. Wolfe St., Park 336, Baltimore, MD 21287. E-mail: jzhou2@jhmi.edu

From the [1]Division of MR Research, Department of Radiology, Johns Hopkins University, Baltimore, Maryland, USA; [2]F.M. Kirby Research Center for Functional Brain Imaging, Kennedy Krieger Institute, Baltimore, Maryland, USA; and [3]Department of Medical Radiation Physics, Lund University, Lund, Sweden

 

standard CEST processing approach of asymmetry analysis, the image has additional signal contributions,[13] in which case "APT-weighted" (APTw) MRI is a more accurate description. APTw MRI has been applied to brain tumors, stroke, and several other diseases. The significance of APTw imaging is that endogenous cellular protein information is obtained indirectly through the bulk water signal used in MRI, thus expanding the range of molecular MRI techniques to the protein level. In this article we review the state of the art of APT-based MRI and the needs for its proper clinical application. In addition, we highlight future prospects of this molecular imaging technique.

## APTw MRI Principles and Techniques

### Basic Principles

The principle of sensitivity enhancement using CEST/APT is explained in Fig. 1a. Low-concentration solute molecules are selectively labeled by saturating specific exchangeable protons (eg, amide, amine, imino, or hydroxyl protons) with radiofrequency (RF) irradiation. When such saturation-labeled protons exchange with water protons, the water signal becomes slightly saturated. In view of the low concentration of solute ($\mu$M to mM range), a single transfer of saturation would be insufficient to show any effect on water protons (100 M range). However, because the water pool is much larger than the saturated solute proton pool, each exchanging saturated solute proton is replaced by a nonsaturated water proton, which is then again saturated. If the solute protons have a sufficiently fast solute-proton to water-proton exchange rate $k_{sw}$ (tens of Hz) and if the $T_1$ of water ($T_{1w}$) is sufficiently long, prolonged irradiation (second range) leads to substantial enhancement of this saturation effect. The magnitude of the CEST effect is generally expressed in terms of a so-called proton transfer ratio (PTR). Based on a two-pool exchange model (small solute pool, large water pool), the amide PTR can be written as[14]:

$$APTR = k_{sw} \cdot ([\text{amide proton}]/[\text{water proton}]) \cdot T_{1w} \cdot \left(1 - e^{-t_{sat}/T_{1w}}\right) \quad (1)$$

where square brackets indicate concentration ([water proton] = 2 × 55.6 M) and $t_{sat}$ is the saturation time, which is the time during which saturation is applied and transfer occurs. Even though most proteins and peptides occur only in $\mu$M concentration in tissue, they contain multiple amide protons. Also, many proteins and peptides can contribute amide groups in vivo at about the same frequency (around 8.3 ppm, or ~3.5 ppm downfield from the water resonance), leading to a large composite resonance reflecting a total proton concentration of about 50–100 mM.[10] Even though the APT effect is small (a few percent on the water signal), it corresponds to a detection sensitivity of molar concentration for millimolar substances.

### APTw MRI-Related Metrics

CEST effects are usually assessed by acquiring a so-called Z-spectrum, in which the intensity of the water signal during saturation at a frequency offset ($\Delta\omega$) from water, $S_{sat}$ ($\Delta\omega$), normalized by the signal without saturation, $S_0$, is displayed as a function of irradiation frequency using the water frequency as a zero-frequency reference (Fig. 1b). When performing an APT experiment in vivo, direct water saturation (DS), and conventional semisolid magnetization transfer contrast (MTC) effects will interfere with the measurement. These effects need to be separated out, which is generally attempted using asymmetry analysis of the Z-spectrum with respect to the water frequency. The sum of all saturation effects at a certain offset is called the magnetization transfer ratio (MTR):

$$MTR(\Delta\omega) = 1 - Z(\Delta\omega) = 1 - S_{sat}(\Delta\omega)/S_0 \quad (2)$$

where $Z = S_{sat}/S_0$ is the signal intensity in the Z-spectrum. The APT effect is usually assessed using the MTR asymmetry at an offset of 3.5 ppm:[10]

$$\begin{aligned} MTR_{asym}(3.5\text{ppm}) &= MTR(+3.5\text{ppm}) - MTR(-3.5\text{ppm}) \\ &= Z(-3.5\text{ppm}) - Z(+3.5\text{ppm}) \\ &= \frac{S_{sat}(-3.5\text{ppm}) - S_{sat}(+3.5\text{ppm})}{S_0} \\ &= APTR + MTR'_{asym}(3.5\text{ppm}), \end{aligned} \quad (3)$$

where $MTR'_{asym}(3.5\text{ ppm})$ is used to describe contributions other than APTR, especially including the exchange-relayed nuclear Overhauser effect (rNOE) of aliphatic protons of mobile macromolecules at –3.5 ppm[15–18] and the inherent asymmetry of the conventional MTC effect.[19] The rNOE is visible in the upfield Z-spectrum at low saturation power and is due to the magnetic interaction between the aliphatic protons in the protein and its exchangeable protons, which then relay the saturation effect to the water signal via exchange. This should not be confused with the semisolid MTC in that spectral region, also an NOE effect of the aliphatic protons, but likely through space directly to bound water. The difference between direct and relayed NOEs can be detected by looking at the pH dependence of the NOE signals, with the rNOE being pH-dependent and the direct through-space NOEs not. Following the most recent literature,[8] we refer to the NOE in mobile macromolecules as rNOE, and the NOE in the semisolid components as MTC.

Because of the presence of these multiple contributions, APT images defined by $MTR_{asym}(3.5\text{ ppm})$ should be called APTw images.[13] It has been demonstrated theoretically[20–22] and with image-directed biopsies[23,24] that $MTR_{asym}(3.5\text{ ppm})$ or APTw is a valid metric for imaging of brain tumors, which was the basis of the first commercial APTw imaging sequence on 3 T clinical MRI scanners.[25] To quantify more pure APT and NOE signals in vivo, several alternative data processing

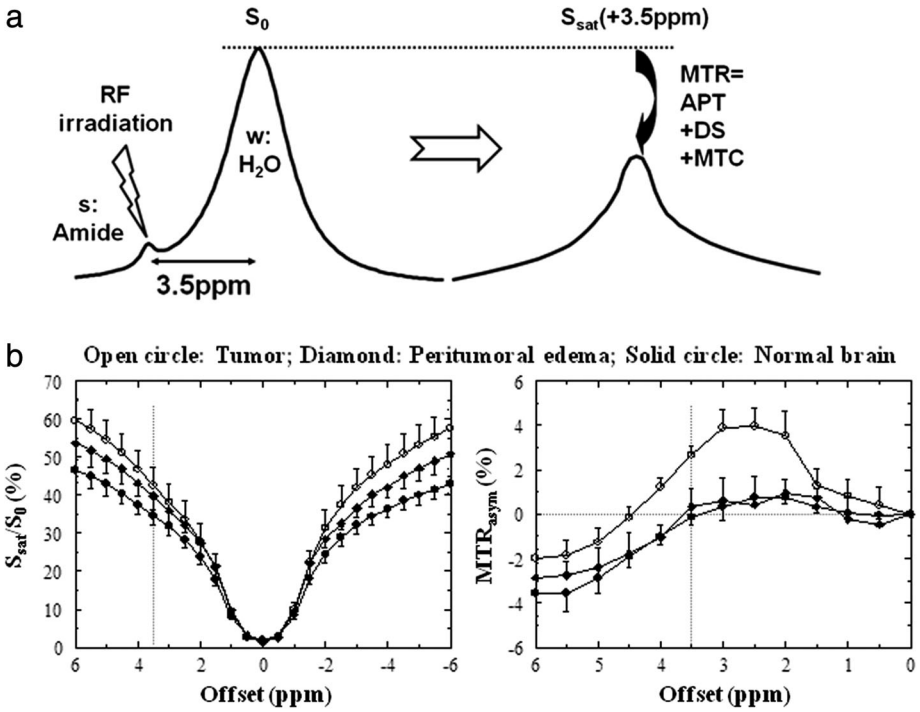


**FIGURE 1: a: CEST/APT detection enhancement principle. The small pool (s) reflects dilute exchangeable amide protons (at ~3.5 ppm downfield of the water resonance) of mobile proteins, and the large pool (w) reflects bulk water protons. The RF irradiation selectively saturates/labels exchangeable protons in pool s, which subsequently exchange with unsaturated protons of pool w (rate $k_{sw}$). b: Z-spectra and $MTR_{asym}$ spectra for tumor, peritumoral edema, and contralateral normal brain tissue in a 9 L tumor rat brain model ($n$ = 5). Compared with the peritumoral edema and contralateral normal brain tissue regions, there is a substantial increase in the tumor $MTR_{asym}$ over the 2–3.5 ppm offset range. Reproduced with permission from Zhou et al, Magn Reson Med 2003;50:1120–1126.**

approaches[21,22,26–31] have been proposed. Many of these are designed to, as much as possible, remove the DS and MTC background signals using some kind of fitting. For example, Heo et al[21,22] recently introduced a mathematical approach, called extrapolated semisolid magnetization-transfer reference (EMR) analysis, in which a limited number of Z-spectrum intensities at large frequency offsets (where no CEST contributions are expected) are used to estimate the reference Z-spectrum of just DS and MTC effects ($Z_{EMR}$). The cleaner APT and NOE results, called $APT^{\#}$ and $NOE^{\#}$, can then be obtained by subtracting the experimentally acquired Z-spectra from the calculated EMR spectra:

$$APT^{\#} = Z_{EMR}(+3.5\text{ppm})\text{-}Z(+3.5\text{ppm}), \quad (4)$$

$$NOE^{\#} = Z_{EMR}(-3.5\text{ppm})\text{-}Z(-3.5\text{ppm}). \quad (5)$$

Quantitative APT MRI with the EMR approach has been shown to achieve more specific APT signals in patients with brain tumors[21,22] and strokes.[32] However, depending on the MTC background fitting approach, the $NOE^{\#}$ signals may still contain some asymmetric MTC in addition to the rNOE contributions. It is expected that quantitative APT MRI has significance for improving the detection accuracy, but this still will have to be validated. Finally, more quantitative image acquisition schemes[33–37] are also being developed. Crucially, the use of MR fingerprinting may achieve absolute CEST parameter quantification for exchange rates and concentrations.[38,39]

### *APTw MRI Pulse Sequences*

Clinical application of the APTw MRI approach requires fast volumetric imaging, either multislice or 3D. Of these, 3D acquisition is preferred to minimize differences in saturation losses caused by $T_{1w}$ relaxation between slices.[40] The most challenging technical problems when designing clinical APTw MRI sequences are strict limitations in the RF amplifier duty cycle and pulse length and in specific absorption rate (SAR).[40–46] This has been addressed by three methods: pulse-train presaturation, pulsed steady-state, or time-interleaved parallel RF transmission (pTX).[47,48] 1) The pulse-train presaturation (a train of pulses separated by brief delays) has been used in some early preclinical APTw studies[10] and in most recent clinical investigations.[40,41,44–46] Notably, Zhu et al[40] developed a 3D APTw MRI technology (Fig. 2) that allows fast acquisition on 3 T clinical instruments, using four elements of 200 msec with 10 msec space in between (duty cycle = 0.95) for gradient- and spin-echo (GRASE) imaging with adiabatic lipid suppression pulses. The SAR of 1.2 W/kg is composed of about 0.8 W/kg from RF saturation and the

remaining from lipid suppression and the multiple refocusing pulses. This sequence has been applied successfully to clinical studies at many sites. 2) In the pulsed steady-state CEST sequence,[49] the CEST effect is built up over multiple saturation pulses, and every short saturation pulse is followed by a segmented imaging readout (including an excitation pulse). 3) To truly maximize the APT effect, a new RF saturation method, the time-multiplexed saturation (alternation) of RF sources in parallel RF transmission (pTX, dual transmit here) systems, was recently introduced by Keupp et al.[47,48] By time-interleaving the two channels, each with a 50% idle-time, one can achieve an arbitrary length of the pseudocontinuous wave (CW) saturation pulse train. The combination of 3D APTw MRI with time-interleaved pTX provides a fast and more sensitive 3D APTw imaging sequence, and is the method used in the first commercial APTw imaging sequence on 3 T clinical MRI scanners.[25]

Currently, there are no consensus-based APTw MRI pulse sequence parameters available for clinical MRI systems from different manufactures. When an RF saturation power ($B_1$) of 2 $\mu$T is used,[50] APTw signal is almost zero for normal brain tissue, due to the presence of a negative $MTR'_{asym}$(3.5 ppm). In addition, the APTw signal should always be negligible in the cerebrospinal fluid. Thus, using this power and sufficient saturation time (0.8–2 sec), the APTw images will be homogenous for most normal brain areas, including the ventricles, allowing detection of hyperintense APTw signals in high-grade tumors or hypointense APTw signals in ischemic tissue. Using a rainbow color scale, this leads to a green background with yellow/orange/red hyperintensities and blue hypointensities, convenient for clinical assessment. A typical CEST MRI acquisition currently requires a relatively long scan time of 5–10 minutes, due to the use of multiple RF saturation frequencies and multiple acquisitions to increase the signal-to-noise ratio (SNR). Recently, several methods have been developed to accelerate CEST/APT acquisitions. These can be classified into conventional fast imaging techniques (such as GRASE[40] and turbo-spin-echo[51]) and reduced *k*-space acquisition techniques (including keyhole,[52] spectroscopy with linear algebraic modeling,[53] variably-accelerated sensitivity encoding,[54] compressed sensing,[55] and snapshot CEST[56]) that require more advanced data processing. We expect the combination of compressed sensing with time-interleaved pTX to become a powerful clinical volumetric APTw imaging method.

### APTw MRI Acquisition Protocols

To identify the APT effect, a full Z-spectrum is often acquired, followed by asymmetry analysis. As the APT signal is known to maximize around 3.5 ppm, in principle only limited saturation images at and around ±3.5 ppm need to be acquired. However, MTR asymmetry analysis is complicated by $B_0$ inhomogeneity, which causes frequency differences between voxels. Any two-offset (±3.5 ppm) APT technique

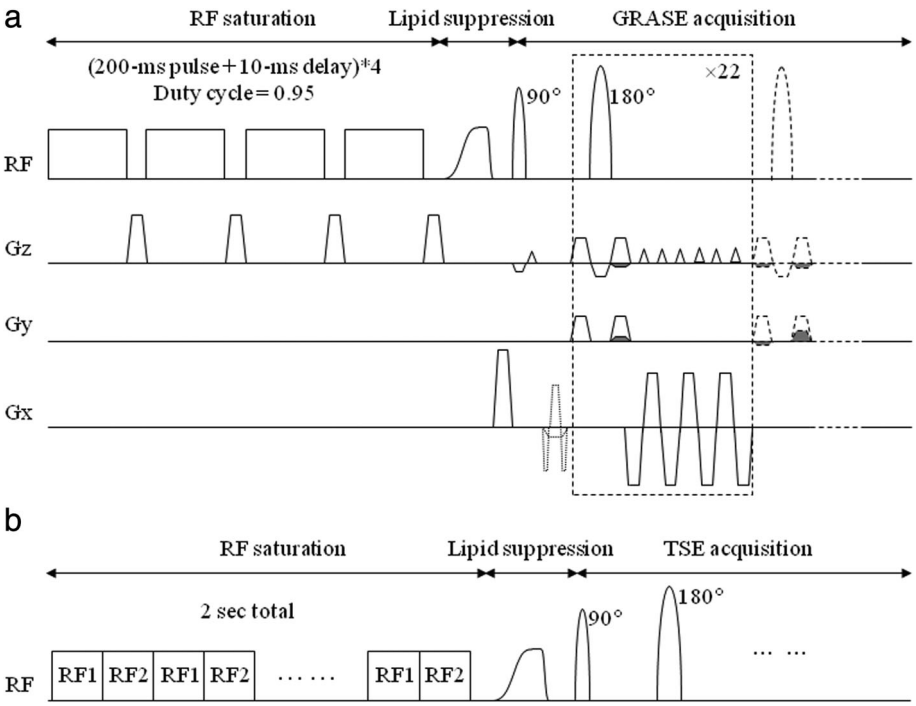


**FIGURE 2: a: 3D APT imaging sequence with gradient- and spin-echo (GRASE) readout. The sequence consisted of four block saturation pulses (200 msec each, 2 $\mu$T), a frequency modulated lipid suppression pulse, and 3D GRASE image acquisition. b: pTX-based, time-interleaved 3D TSE APT sequence. The RF saturation ($t_{sat}$ = 2 sec) consisted of 40 time-interleaved block pulses on two RF transmit channels (50 msec duration each; 2 $\mu$T amplitude). Reproduced with permission from Zhu et al, Magn Reson Med 2010;64:638–644.**

is dependent on proper centering of the water frequency and thus good $B_0$ homogeneity, which can be problematic near air–tissue interfaces. Thus, linear and second-order shimming is always very helpful for APTw imaging. To correct remaining $B_0$ inaccuracies on a voxel-by-voxel basis, it is necessary to acquire multiple offsets around ±3.5 ppm and a water frequency reference map (Fig. 3). As the APTw effect in vivo is often small (2~3% of the water intensity in tumors), multiple acquisitions for each offset are often needed to increase the SNR to at least ~50:1. A recent study showed that the use of three offsets around ±3.5 ppm and several acquisitions provided $B_0$ inhomogeneity-corrected APTw images of sufficient SNR.[13]

Water frequency mapping can be achieved using the water saturation shift referencing (WASSR[57]) method that provides sub-Hertz accuracy for spectral frequency alignment. In this approach, a pulse sequence similar to the APT scan is used, but with low $B_1$ and short saturation duration (for example, 0.5 $\mu$T and 100 msec), which produces a Z-spectrum dominated by direct saturation. Because the shape of this saturation line is a Lorentzian, the water center frequency can be determined using either symmetry analysis[13] or Lorentzian fitting.[58] WASSR can be done much faster than APT due to lower power deposition (less than 1 min). Corrections for $B_0$ field inhomogeneity in CEST imaging can also be done with gradient-echo methods.[51,59] Notably, Keupp et al[60,61] developed a so-called CEST-Dixon method that provides an intrinsic assessment of the $B_0$ inhomogeneity during the APT acquisition. Intrinsically referenced APT methods are more robust than separate $B_0$ mapping approaches, because the obtained homogeneity information reflects the magnetic field during the actual APT acquisition. Note that Z-spectral acquisition at lower $B_1$ values provides an intrinsic $B_0$ frequency reference through the well-defined water signal. At higher fields, the homogeneity of the $B_1$ field becomes a concern. To address this, a combined $B_1/B_0$ fitting approach was recently developed.[62]

## Current Applications

### *Brain Tumors*

Currently, the most-used application of APTw MRI is for the study of brain tumors, where it is starting to impact brain tumor detection, grading, the assessment of recurrent tumor vs. treatment effects, and the identification of tumor genetic markers. The added value of APTw MRI in enhancing the noninvasive molecular diagnosis of brain tumors can potentially aid in guiding brain tumor therapies, such as surgery, radiotherapy, and local chemotherapy.

*DETECTING TUMORS.* Standard MRI sequences (such as $T_2$w, FLAIR, and Gd-$T_1$w) are not sufficiently tissue-specific and suffer from several limitations. For example, when diagnosing malignant gliomas, $T_2$w hyperintensity may represent both infiltrating tumor and peritumoral vasogenic edema. Gadolinium enhancement reveals focal areas of malignant gliomas where the blood–brain barrier is disrupted, but it does not show all infiltrating tumor areas with high cellularity and proliferation or may enhance some low-grade tumors, leading to erroneous diagnosis.[63] Therefore, standard MRI is often inconclusive with regard to actual tumor locations needed for successful surgery or other local therapies. There are numerous ongoing investigations about the ability of functional and

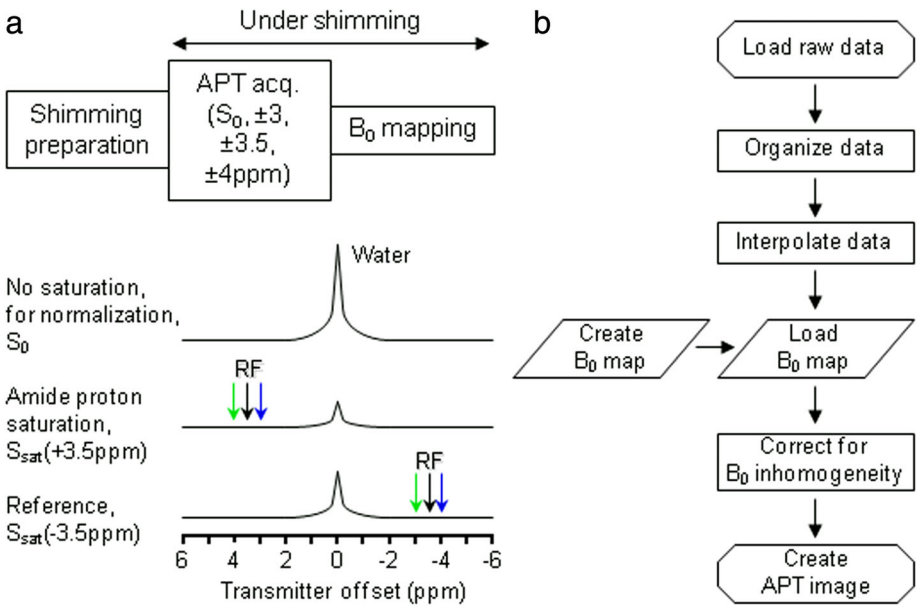


**FIGURE 3: a: Six-offset APT data acquisition protocol with shimming typically up to the second order. During the APT data acquisition, extra offsets (±3, ±4 ppm) are acquired to correct for the residual $B_0$ inhomogeneity. b: APT data processing flow chart. The procedures include the generation of $B_0$ shift map and correction of APT data using $B_0$ map. Reproduced with permission from Zhou et al, Magn Reson Med 2008;60:842–849.**

molecular MRI approaches to assess brain tumor burden.[64] The APTw MRI technology for imaging of brain tumors was introduced in 2003.[65] Data on several rodent tumor models (such as 9 L gliosarcoma, U87MG glioma, SF188/V+, and human glioblastoma xenografts from resected tumors)[65–67] clearly showed that a high APTw signal is detected in tumors. APTw imaging was applied to brain tumor patients 3 years later,[13,68] confirming increased APTw signal in high-grade tumors (Fig. 4) relative to peritumoral edema and contralateral brain. Actually, the hyperintense regions on APTw images are sometimes larger than the areas of contrast enhancement on Gd-$T_1$w images, but smaller than the abnormal areas designated as tumor on $T_2$w, $T_1$w, and FLAIR. Numerous studies from different institutions[69–74] indicate that APTw imaging may add important value to brain cancer diagnosis.

A brain tumor is highly cellular, and many proteins are overexpressed compared with normal brain tissue, which was the original hypothesis for APTw hyperintensity based on MR spectra of perfused tumor cells.[12] Theoretically, the APTw hyperintensity in glioma can be caused by increased cytosolic protein content or increased intracellular pH.[14] In this respect, it is worth mentioning that there was no correlation between the amide proton exchange rate and extracellular pH measured in an exogenous contrast agent-based CEST experiment (acidoCEST).[75] As shown recently,[14,76] the increased protein content in the tumor is the most likely explanation, because only a small intracellular pH increase (<0.1 unit) is often detected. The results are consistent with increasing protein concentrations in malignant tumors, as revealed by MRI-guided proteomics[77,78] and in vivo MR spectroscopy.[79] In any event, an intracellular increase in pH would be synergistic for tumor detection. Note that extracellular pH tends to be acidic due to lactate removal from the cell,[80] suggesting that the proteins and peptides of interest for the APTw contrast are located predominantly inside the tumor cell, as the amide exchange rate reduces substantially at lower pH. Another possible contribution to increased protein signal in malignant tumors is angiogenesis, as the blood contains high concentrations of hemoglobin and albumin.

*GRADING TUMORS.* The early clinical results on 3 T clinical MRI scanners from several labs[23,81–88] show that APTw hyperintensity (either ring-like or nodular) is a typical feature of high-grade gliomas (grades III and IV). Gadolinium-enhanced MRI is limited in that some high-grade gliomas (roughly 10% of glioblastomas and 30% of anaplastic astrocytomas[89]) demonstrate no gadolinium enhancement. In addition, gadolinium enhancement is not always specific for tumor grade, as low-grade gliomas occasionally enhance.[90] Therefore, it is an important feature that, in cases with high-grade gliomas without gadolinium enhancement, APTw-hyperintense foci are still clearly visible within the lesions.[81] Notably, a recent study using APTw image-guided stereotactic biopsy by Jiang et al[23] suggests that APTw imaging can identify high-grade regions within heterogeneous gliomas, allowing more precise sampling of the highest-grade region of a tumor. On the other hand, in patients with

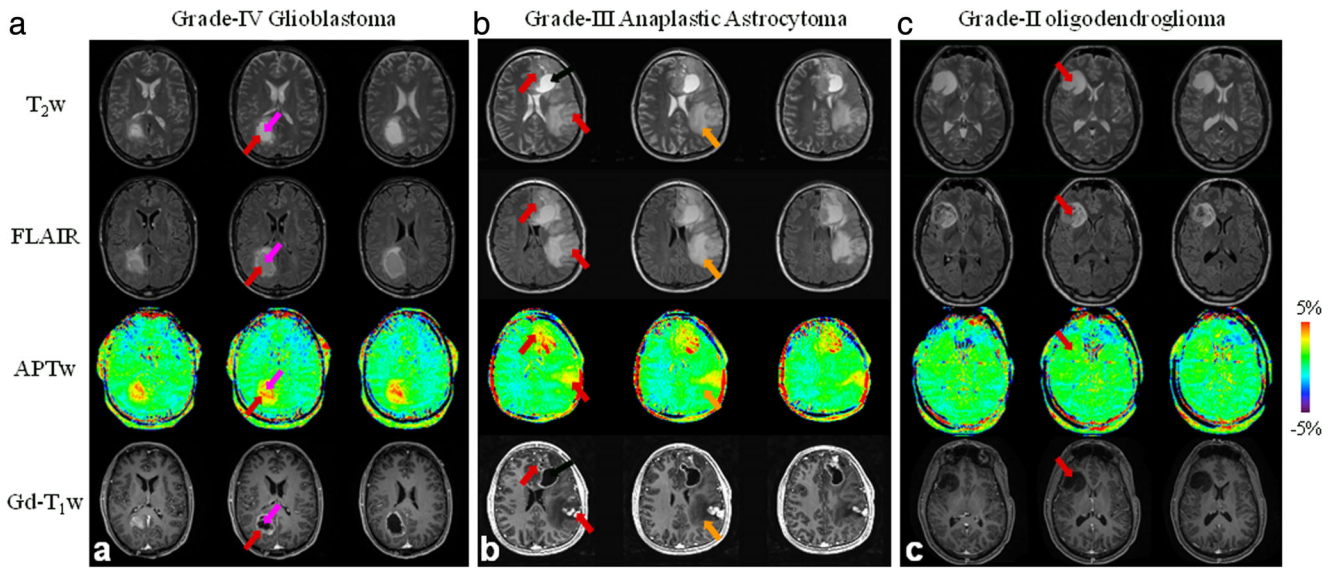


**FIGURE 4: a: APTw and conventional MR images for a patient with a glioblastoma. APT-weighted image shows hyperintensity in the gadolinium-enhancing area (red arrow) and in the centrally cystic area (back arrow), compared with the contralateral brain area. b: APTw and conventional MR images for a patient with a multifocal grade-3 anaplastic astrocytoma. APT imaging shows that the tumor cores are hyperintense. c: APTw and conventional MR images for a patient with a low-grade glioma. APTw image shows isointensity in the lesion, compared with the contralateral brain tissue. Areas of gadolinium enhancement, FLAIR hyperintensity, and APTw hyperintensity are unique from one another, and APTw imaging adds new information to the standard MRI techniques. Red arrow: tumor core; orange arrow: peritumoral edema. The APTw scan time is 8 minutes, 10 seconds. Three of 15 slices are shown. (a,c) Reproduced with permission from Zhou et al, J Magn Reson Imaging 2013;38:1119–1128.**

pathologically confirmed low-grade gliomas, including those with gadolinium enhancement, APTw imaging shows isointensity or scattered punctate hyperintensity within the lesion. These initial findings, confirmed by different researchers,[23,81–88] indicate that APTw imaging for malignant brain tumors has the unique potential to become a valuable imaging biomarker for separating high- from low-grade gliomas and to detect high-grade tumors that do not show gadolinium enhancement or false-positive low-grade tumors that enhance.

*DISTINGUISHING ACTIVE GLIOMA FROM TREATMENT EFFECTS.* A major obstacle in the daily management of patients with malignant gliomas and many other cancers is the inability of most currently available imaging techniques to accurately assess tumor response to therapy.[91] In a preclinical APTw MRI study of models of radiation-induced necrosis in rats, Zhou et al[92] showed that regions with radiation necrosis appeared hypointense or isointense with respect to normal-appearing contralateral tissue. The interpretation was that such necrotic lesions are associated with the absence of mobile cytosolic proteins due to the loss of the cytoplasm and organelles, thus showing a low APTw signal. When assessing radiation treatment in glioma models, the irradiated tumors appeared to enlarge during the first several days postradiation as judged from $T_2$w MRI, while their APTw signals gradually decreased. This and further studies have shown that APTw imaging provides a unique imaging method for evaluation of tumor response to radiotherapy,[92–94] chemotherapy,[95] and high-intensity focused ultrasound therapy.[96]

Several clinical studies have now confirmed the ability of APTw imaging to differentiate recurrent tumor from treatment effects.[24,97–101] These early results demonstrate the potential of APTw imaging in neuro-oncology, providing a noninvasive imaging biomarker for distinguishing active tumor from radiation necrosis. For example, Zhou et al applied a 3D APTw sequence to patients with clinically suspected tumor progression after chemoradiation.[97,98] It was found (Fig. 5) that true progression was associated with APTw hyperintensity, while pseudoprogression was associated with APTw isointensity to mild hyperintensity. A recent radiographically guided stereotactic biopsy study showed that APTw signal intensities were significantly higher in regions that represented active tumor than in regions that represented nonactive tumor, and that these two groups could be separated with an 85.1% sensitivity and a 94.1% specificity.[24] This further supports the hypothesis that the APTw hyperintensity for active glioma can be used as a surrogate biomarker to differentiate recurrent tumor from treatment effects. Currently, posttreatment patients with suspected recurrence are often referred for repeated surgery to obtain pathologic confirmation of active cancer, and APTw MRI may assist in the

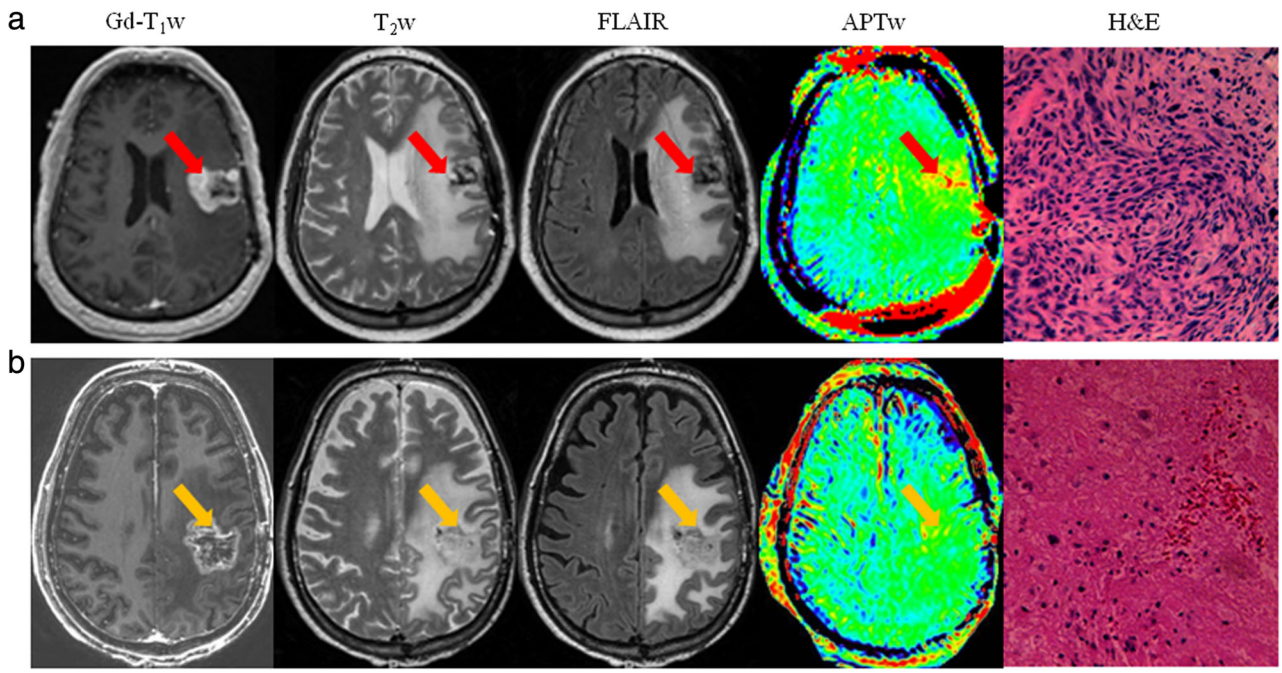


**FIGURE 5: a: Conventional and APTw MRI and histology from a patient with tumor progression. The gadolinium-enhancing areas on Gd-$T_1$w were hyperintense on the APTw images, compared with the contralateral brain area. Hematoxylin and eosin (H&E)-stained section demonstrated spindle mesenchymal cell proliferation with segregated glial cells. b: Conventional and APTw MRI and histology from a patient with a clinical diagnosis of pseudoprogression. The gadolinium-enhancing lesion appeared isointense on APTw, with punctate APTw hyperintensity scattered within the lesion. H&E-stained section showed large necrosis with scattered dying tumor cells and inflammatory cells. For APTw images (display window –5% to 5%), 15 slices were acquired, and only one is shown. Reproduced with permission, and with the addition of pathology images, from Ma et al, J Magn Reson Imaging 2016;44:456–462.**

accurate targeting of the most malignant regions of tumor during neurosurgical procedures in the short term. Notably, APTw imaging has the potential to improve the noninvasive differential diagnosis of these two pathologies. In the long term, this could potentially reduce the necessity for repeated biopsies, thus avoiding the associated risks of complications.

*IDENTIFYING GENETIC MARKERS IN GLIOMAS.* The most recent 2016 WHO classification of central nervous system tumors, in addition to histology, uses molecular markers such as isocitrate dehydrogenase (IDH)1/2 mutation and 1p/19q codeletion to define tumor entities.[102] These new guidelines address an unmet radiographic need, namely, the ability to identify genetic biomarkers preoperatively. Until now, MRS has been the only in vivo method with which to assess IDH mutation status through measurement of 2-hydroxyglutarate (2-HG) levels.[103] However, the MRS detection of 2-HG in IDH-mutant gliomas requires a large tumor volume,[104] and is time-consuming, which limits its clinical application. In two recent retrospective studies, Jiang et al have shown that the APTw signal has potential as an imaging biomarker for identifying IDH mutation status in low-grade gliomas and MGMT methylation status in high-grade gliomas.[105,106] These preliminary APTw MRI results showed that IDH-wildtype lesions were typically associated with relatively high APTw intensities, compared with IDH-mutant lesions. This is consistent with lab research results, showing global downregulation of protein expression in mutant IDH1-driven glioma cells, compared with oncogenic HRAS IDH1-wildtype glioma cells.[107] These early findings, together with some recent confirmatory results,[108,109] are very promising. If these APTw results are validated in rigorous clinical studies, the preoperative determination of genetic biomarkers can potentially be done rapidly and noninvasively.

## Stroke

There are two major types of stroke: ischemic and hemorrhagic. The intrinsic nature of the APTw MRI in terms of being pH-sensitive and providing information about protein content allows this contrast to be used to simultaneously assess pH changes during early ischemia and the leakage of blood into tissue during hemorrhage.

*DETECTING ISCHEMIC STROKE.* The only current treatment for ischemic stroke is to remove blockages to brain tissue regions that are still viable, but at risk of infarction without restoration of blood flow. These areas constitute what is commonly referred to as the ischemic penumbra.[110] Using MRI, a spatial mismatch between abnormal areas on diffusion-weighted imaging (DWI; mostly, but not always, progressing to infarction) and perfusion-weighted imaging (PWI) has long been proposed as a surrogate marker for identifying an ischemic penumbra, but this concept has turned out to be flawed due to the presence of oligemia in large parts of the mismatch.[111–113] Because anaerobic metabolism and acidification of tissue are considered the first sign of tissue at risk, it is expected that APT-based pH imaging could provide the missing marker that can be used for subdividing the DWI-PWI mismatch into areas of oligemia and acidosis, thus allowing more accurate diagnosis and prognosis of acute stroke patients.[114] Zhou et al[10] first demonstrated the existence of pH-sensitive APT effects in a rat global ischemia model in 2003. They found reduced $MTR_{asym}$(3.5 ppm) in postmortem brain, which was attributed to the slower exchange induced by pH reduction. In the case of ischemia, the $MTR_{asym}$(3.5 ppm) images calculated from Eq. [3] have been called pH-weighted (pHw) images. By using $^{31}P$ spectroscopy for pH assessment (pH 7.11 in vivo vs. 6.66 postmortem), they calibrated the change in APTR in a global ischemia model to be:

$$APTR = 5.73 \times 10^{pH-9.4} \quad (6)$$

Using Eq. [6], an absolute pH image could be generated in the rat brain following permanent middle cerebral artery occlusion (MCAO),[10] correctly outlining an ischemic area in the caudate nucleus with an average pH of 6.52 $\pm$ 0.32 ($n$ = 7). Sun et al investigated the use of pH-based APT MRI to detect an acidosis-based penumbra.[115] They imaged adult rats with different severities of permanent MCAO using multiparametric MRI over the first 3.5 hours postocclusion. In all rats, while the large MCA perfusion territory showed hypoperfusion on cerebral blood flow (CBF) images, no $T_1$ and $T_2$ changes were found during this period. Notably, several animals showed negligible apparent diffusion coefficient (ADC) effects in the hyperacute period, despite the presence of pH effects, confirming that pH changes occur before ADC changes, as expected from the ischemic flow thresholds. Importantly, the pH-based penumbra correctly predicted the infarcted region measured by $T_2$w MRI after 24 hours. These data confirmed the presence of a hypoperfused area with a decrease in pH without an ADC abnormality, corresponding to an ischemic acidosis penumbra, as well as a hypoperfused region at normal pH, corresponding with benign oligemia. APTw imaging of permanent and reversible brain ischemic models has been intensively studied over the past 12 years, confirming these early established principles.[116–123]

These promising results stimulated efforts to translate this work to the clinic.[50,124–126] For instance, in a recent prospective study of 12 patients with acute ischemic stroke, Harston et al[125] showed that voxels within the ischemic core had a more severe intracellular acidosis than hypoperfused tissue recruited to the final infarct (ischemic penumbra), which in turn was more acidotic than hypoperfused tissue that survived (benign oligemia). Moreover, when confined to the gray

matter perfusion deficit, intracellular pH, but not CBF, differed between tissue that ultimately infarcted and tissue that survived. However, contrary to the brain tumor work, the effect size of the APTw MRI signal changes has always been quite small and, although promising, never very convincing. Recently, it has become better understood that this dilemma is due to the use of the $MTR_{asym}$(3.5 ppm) approach, where the APT and rNOE intensities are subtracted. While these two effects act synergistically and add up in the APTw MRI contrast of brain tumors due to the considerable MTC asymmetry at higher $B_1$,[20–22] they do not for pH assessment in ischemic stroke, where the pH dependence of the rNOE effect compensates a part of the pH dependence of the APT signal. To address this and illustrate the detrimental effect of the $MTR_{asym}$(3.5 ppm) approach, Heo et al[32] performed a study in ischemic stroke patients using the EMR approach, confirming pH effects in both quantitative $APT^{\#}$ and $NOE^{\#}$ images. Use of the more specific $APT^{\#}$ images showed a great enhancement of the APT MRI sensitivity to pH compared with conventional APTw MRI (Fig. 6), allowing a more reliable delineation of the acidosis penumbra.[32] It is expected that the pH/diffusion mismatch will be better than the current standard of care criteria (perfusion/diffusion mismatch) at identifying the true viable tissue area at risk of infarction, ie, the ischemic penumbra. This may help avoid unnecessary treatment, and perhaps allow recommendation of stroke patients for treatment at longer times postictus, even later than the current therapeutic window.

*DIFFERENTIATING ISCHEMIA FROM HEMORRHAGE.* Accurate early detection of hemorrhagic stroke with neuroimaging is crucial for all stroke patients. In the clinic, this is achieved with computed tomography, but it has been demonstrated recently[127] that APTw MRI can also be used to identify intracerebral hemorrhage (ICH) and to differentiate between ICH and ischemia at the hyperacute stage in rat models. Notably, APTw MRI showed opposite contrast between ICH (hyperintense compared with the contralateral brain tissue) and cerebral ischemia (hypointense) at each timepoint during the hyperacute stage. In hyperacute hemorrhage, the hematoma following vessel rupture consists of a collection of red blood cells (which are rich in hemoglobin content), white blood cells, platelet clumps, and albumin-rich serum. It was therefore concluded that the hyperintensity in the hyperacute hemorrhage APTw signal reflects the presence of abundant mobile proteins and peptides. APTw hyperintensities in blood have also been reported in pure blood samples and blood vessels[128] and in many brain lesions.[67,69,129] Notably, APTw MRI has recently been applied to detect ICH at the hyperacute, acute, and subacute stages in the clinical setting.[130] These results suggest that APTw MRI has potential to detect and distinctly differentiate hyperacute ICH from cerebral ischemia, thus opening up the possibility of introducing to the clinic a single MRI scan for the simultaneous visualization and separation of hemorrhagic and ischemic lesions at the hyperacute stage.

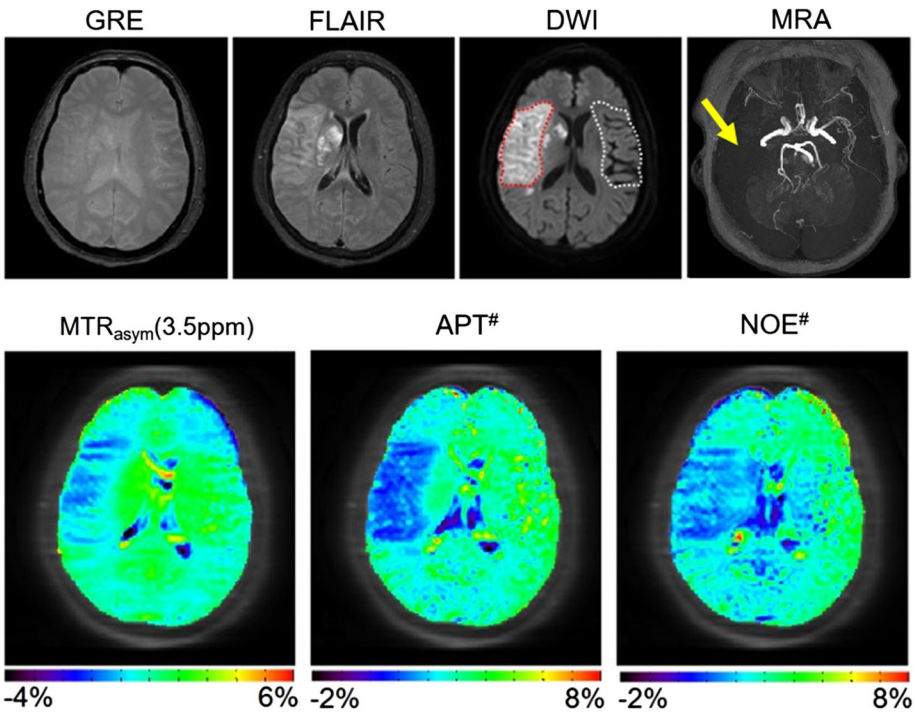


**FIGURE 6: APTw imaging of an acute stroke patient with right MCA occlusion (<7 hours from symptom onset) using the MTR asymmetry analysis and EMR approaches. $APT^{\#}$ and $NOE^{\#}$ showed much clearer ischemic contrasts than $MTR_{asym}$(3.5 ppm). Reproduced with permission from Heo et al, Magn Reson Med 2017;78:871–880.**

### Other Neurological Applications

Alzheimer's disease (AD) is an age-related, nonreversible brain disorder characterized by accumulation of extracellular amyloid plaques and intracellular neurofibrillary tangles. In a recent study, Wang et al[131] tested the feasibility of APTw imaging for detecting cerebral abnormality in AD patients and for discriminating patients with different disease severity. Bilateral hippocampal APTw MRI showed a consistent trend of increasing hyperintensity from controls to mild AD, to moderate-severe AD. The APTw values were significantly negatively correlated with mini-mental state examination (MMSE) scores (right $r$ = –0.602, left $r$ = –0.536, both $P < 0.001$). These preliminary results suggest that APTw imaging may be valuable to detect early AD and to monitor the disease progression noninvasively.

Parkinson's disease (PD) is a neurodegenerative disease characterized by a decreased dopamine level in the dopaminergic neurons in the substantia nigra.[132] The diagnosis of PD, especially at an early stage, remains challenging. Li et al[133,134] tested the feasibility of APTw imaging in PD patients at a field strength of 3 T (Fig. 7). In regions of the substantia nigra and red nucleus, the APTw signal intensities were reduced in patients vs. normal controls (even though insignificantly for the red nucleus). Quantitatively, the CEST signal intensities in the substantia nigra showed a consistent trend of lower hypointensity from normal controls to early-stage PD, to advanced-stage PD. Moreover, for PD patients with unilateral symptoms, the APTw intensities in the substantia nigra on the affected side were significantly lower than those in normal controls.[135] On the contrary, in regions of the globus pallidus, putamen, and caudate, the APTw signal intensities were increased in PD patients. It was hypothesized that the loss of dopaminergic neurons is associated with reduced CEST signal in the substantia nigra of PD patients, while accumulation of abnormal cytoplasmic proteins (such as α-synuclein) is associated with high APTw signal in some other areas (such as striatum).[136,137] These and the AD results show that APTw imaging has potential as an imaging biomarker that could detect neurodegenerative disease and predict its progression.

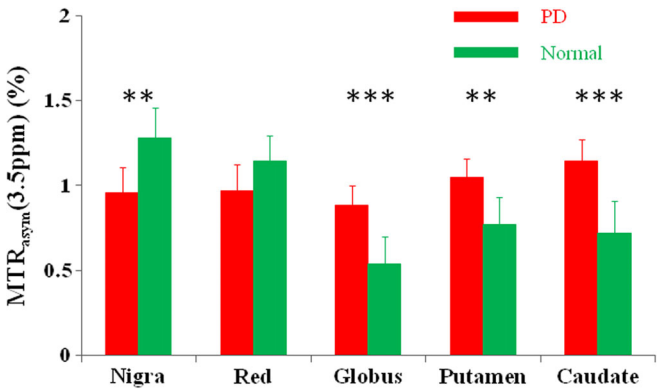


**FIGURE 7: Comparison of the average $MTR_{asym}$(3.5 ppm) signals of the substantia nigra, red nucleus, globus pallidus, putamen, and caudate for Parkinson's disease (PD) patients ($n$ = 27) and normal controls ($n$ = 22). In regions of the substantia nigra and red nucleus, the $MTR_{asym}$(3.5 ppm) signals were reduced in PD patients, compared with normal controls. In regions of the globus pallidus, putamen, and caudate, the $MTR_{asym}$(3.5 ppm) signals were increased in PD patients, compared with normal controls. Reproduced with permission from Li et al, Eur Radiol 2014;24:2631–2639.**

Multiple sclerosis (MS) is a neurodegenerative disease characterized by chronic inflammation of the central nervous system and the occurrence of plague-like lesions in multiple tissues, especially white matter due to demyelination that may later progress to axonal damage.[138] Preliminary reports of APTw MRI in MS patients in the brain[139] and the spine[140] performed with different saturation settings showed great variability in the results, with increased APTw intensity found in some brain and spine lesions but an overall histogram shift to lower APTw intensity in lesions of spine white matter. Increases in APTw MRI were suggested to possibly be due to protein degradation increasing the content of smaller mobile proteins, but the overall conclusion was that more studies are needed. The investigation of magnetization transfer phenomena in MS is complicated by a reduction in MTC due to demyelination and an overall reduction of Z-spectral intensity in lesions with increased water content. Thus, future studies have to be carefully designed to rule out such contributions.

Traumatic brain injury (TBI) may result in primary (such as contusion, hemorrhage, and diffuse axonal injury) and secondary (such as cerebral ischemia, excitotoxicity, oxidative stress, inflammation, and edema) injury cascades. In a recent study on adult rats subjected to controlled cortical impact-induced severe TBI at 4.7 T, Zhang et al[141] demonstrated unique APTw MRI signal characteristics at different timepoints after injury (Fig. 8), which were associated with ischemia (decreased pH due to tissue acidosis, showing hypointensity with respect to contralateral normal tissue); hemorrhage (increased concentration of endogenous mobile proteins and peptides, showing hyperintensity); or neuroinflammation (increased inflammatory cell density, showing hyperintensity). Notably, unlike many currently used advanced MRI techniques, APTw MRI can provide visual interpretation (not just statistical differences in image analysis) for these key TBI pathophysiological features. Subsequently, Wang et al[142] further examined the treatment efficacy of pinocembrin, a natural antiinflammatory and neuroprotective compound. They found that, at 3 days post-TBI, the APTw signals in the ipsilateral cortex and hippocampus increased significantly in the TBI group compared with the sham group, but significantly decreased in the TBI + pinocembrin group, compared with the TBI group. Further immunofluorescence data showed a similar trend. These early data suggest that the APTw signal could be a sensitive imaging biomarker of neuroinflammation and an antiinflammatory response in TBI that can potentially be used to evaluate treatment efficacy objectively and reliably.

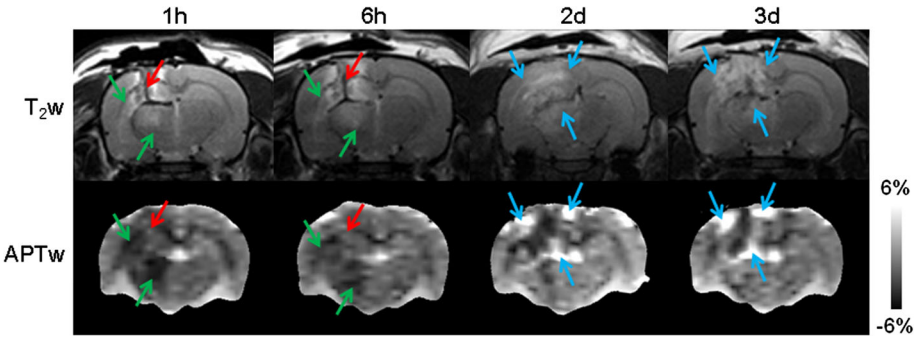


**FIGURE 8: A typical example of $T_2$w and APTw images of TBI in a rat at different timepoints. Green arrows: ischemia; red arrows: hemorrhage; blue arrows: inflammatory response (increased inflammatory cell density). Reproduced with permission from Zhang et al, J Cereb Blood Flow Metab 2017;37:3422–3432.**

## Challenging Issues and Controversies

There are several challenging issues for clinical APT-based imaging, some similar to conventional MTC imaging. These issues include scanner RF amplifier constraints, SAR requirements, long scan time, complicated contrast mechanism with multiple contributions, data interpretation depending on the scan parameters used, and the possibility of $B_0$ inhomogeneity artifacts and lipid artifacts.

### *Scanner Hardware*

For APTw imaging on animal systems, RF saturation is typically applied using a CW block pulse of several seconds to maximize effects. However, clinical MRI systems generally have limited amplifier duty-cycles and saturation pulse lengths, especially due to the use of large body coils for transmit.[40–46] Due to a lack of agreed-upon standards between the research community and manufacturers, current APTw and other CEST imaging protocols are generally "works in progress" and vary substantially among different institutes, far from being optimized, and the results acquired from different research centers are often difficult to compare. Currently, the recommended RF power for APTw imaging of brain tumors is about 2 $\mu$T with a total RF saturation time of about 0.8–2 seconds (possibly with interpulse delays) to generate a homogeneous background signal for normal brain tissue (see above for the reason for this choice).[50] Without this, the proper APTw contrast may not be obtained, and results may vary strongly with respect to published literature.[43,143]

The ultimate goal for APT-based imaging is reproducible clinical use on a variety of MRI systems from different vendors. Thus, there is an urgent need for industry and academia to work together to develop this emerging technology into a clinically viable, easy-to-use, optimized, and standardized approach. In this respect, it is encouraging to see that the recent 7$^{th}$ International Workshop on CEST Imaging featured a special session discussing standardization involving the three main MRI vendors, illustrating that this is a high priority for this community.[144] The APTw imaging sequence is now available commercially as a product sequence through one vendor,[25] and we are looking into working with these vendor-supplied sites to set up a clinical trial. The other vendors have "works in progress" packages, which should be run with the optimized parameters mentioned above. Thus, more medical centers will soon be able to utilize the technique in daily clinical practice and to explore new applications on all fronts.

### *APTw MRI Signal Contributions*

Many studies in animal models and humans have clearly shown that APTw signals are higher in tumor core than in peritumoral edema and in normal tissue. Theoretically, APTw imaging detects mobile proteins and peptides in tissue (such as cytosolic proteins, many endoplasmic reticulum proteins, and secreted proteins[78]), while conventional MTC detects semisolid macromolecules (including proteins and lipids). The physical mechanisms that underlie conventional MTC imaging and APTw imaging have been compared recently.[8] With respect to mobile proteins and peptides, the composite CEST peak of finite width around +3.5 ppm (namely, APT) is attributed to the backbone amide protons (Fig. 9). In addition, guanidinium protons of protein sidechain arginine groups as well as creatine contribute to another CEST peak at 2 ppm.[65,145] It is important to understand that CEST experiments detect only certain protons in certain proteins, depending on the water accessibility and mobility. Therefore, total cellular protein concentration measurements are not representative of what is measured in APTw experiments and thus should not be used to interpret those results. Notably, as shown in a recent study using the rat 9 L tumor model,[78] the total protein concentrations in the tumor and normal brain tissue were comparable, but there was a significant increase in the assessed mobile protein concentration in the tumor, based on the increased APTw intensity.

The standard APTw MRI metric, $MTR_{asym}$(3.5 ppm), is based on the mixing of multiple contributions to the water Z-spectrum, each of which depends in magnitude on the experimental saturation parameters (length, $B_1$, and shape of the RF pulses, and the interpulse spacing). In the brain, the downfield (high frequency, $+\Delta\omega$) side of the water Z-spectrum consists of contributions of all exchangeable protons

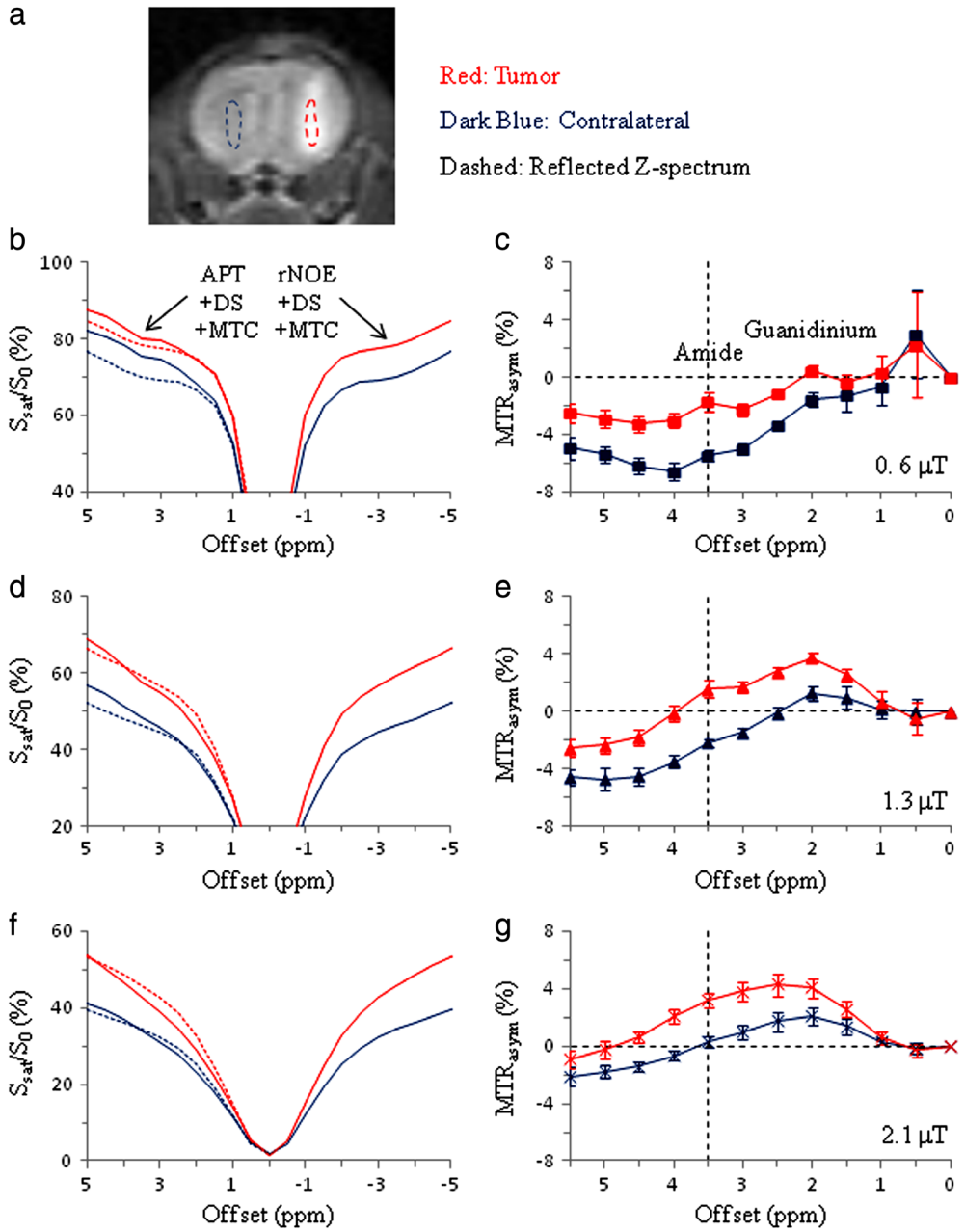


**FIGURE 9: Average Z-spectra and $MTR_{asym}$ spectra of brain tumors and contralateral normal brain tissue in a rat 9 L gliosarcoma model ($n$ = 8) at 4.7 T obtained at three different RF saturation powers and $t_{sat}$ = 4 sec. a: Regions of interest (ROIs) for the image analysis defined on an MT-weighted image at 6 ppm. b,c: $B_1$ = 0.6 $\mu$T. The downfield Z-spectra of the tumor and contralateral normal brain tissue are both higher than the corresponding reflected Z-spectra. d,e: $B_1$ = 1.3 $\mu$T. f,g: $B_1$ = 2.1 $\mu$T. At 3.5 ppm (use green dashed vertical guideline), the tumor Z-spectrum is lower than the corresponding reflected Z-spectrum, while the contralateral downfield Z-spectrum is about equal to the corresponding reflected Z-spectrum. Reproduced with permission and with some additions from Zhou et al, Magn Reson Med 2013;70:320–327.**

(CEST/APT), DS, and semisolid tissue components (MTC), while the upfield (low frequency, $-\Delta\omega$) side, in addition to DS, has aliphatic NOE-based signals of mobile (rNOE) and semisolid (MTC) proteins and lipids. The relative contributions of these effects are a function of the pulse sequence parameters and the magnetic field strength $B_0$, and, to make matters worse, these effects mix when performing an asymmetry analysis. The principle that plays a role becomes clear when looking at some data from a recent study[20] in rat brain tumors using CW saturation at 4.7 T (Fig. 9). At low power (0.6 $\mu$T) in vivo, the sum of all upfield saturation effects (rNOE+DS + MTC) in normal brain at 3.5 ppm is much larger than the sum on the other side downfield with respect to water (APT+DS + MTC), while the magnitude of these saturation effects in tumor is about comparable. The most likely interpretation is that the semisolid MTC asymmetry due to myelin lipid chains is removed in the tumor due to white matter being replaced with tumor cells. At relatively high power (2.1 $\mu$T) in vivo, the result is about the opposite, in that the upfield saturation effect in normal brain at

3.5 ppm is approximately equal to the downfield saturation effect, while the magnitude of these two effects in tumor is very different. While the increased symmetric effect of DS at high $B_1$ flattens the spectrum, we attribute the larger downfield saturation to the increased APT effect, likely due to the contribution of relatively faster exchanging amide protons in proteins and peptides.[146] Thus, we may conclude that the $MTR_{asym}$(3.5 ppm) at low $B_1$ has a large contribution from the original tissue MTC asymmetry, while at higher power it is dominated by the APT effect. Importantly, this interpretation was indirectly confirmed in an egg white experiment,[20] showing that rNOE and APT effects were about equal at 0.6 $\mu$T (giving negligible asymmetry), while at 2.1 $\mu$T the effect of amide protons (and potentially guanidinium and amine protons with broad resonances) was much higher than the rNOE. Interestingly, the $MTR_{asym}$(3.5 ppm) difference between tumors and normal brain tissue remains about the same at different $B_1$ (Fig. 9), but the signal origin is very different, impacting the mechanistic interpretation when performing in vivo experiments.

These differences in APTw contrast contributions as a function of experimental conditions have led to some controversy in the literature when comparing results between labs that used very different pulse sequences and parameters (particularly saturation time and power)[43,143] and sometimes data analysis approaches (see below). For instance, dominance of one type of contribution (eg, rNOE/MTC asymmetry vs. APT) has sometimes been concluded in one lab and the opposite in another, making the literature confusing and leading to scientific arguments that can easily be avoided. Therefore, rather than generalizing conclusions in a way that all APTw experiments seem equal, it is crucial to carefully document and discuss the approaches used, thus allowing readers of these publications to better understand the origin of the particular APTw contrast found and the approach-specific conclusions reached. Based on the currently available literature for APTw MRI of tumors, we recommend using a $B_1$ of about 2 $\mu$T and a $t_{sat}$ of 0.8 sec or more. Figures 4–6 show some examples of these parameters in a human study at 3 T, confirming the minimizing of normal tissue and edema signal into the background and a strong tumor contrast. These saturation parameters were also used in the validation studies with APTw MRI-directed biopsies.[23,24] For other applications, the optimal parameters and analysis approaches are still under development.

### Quantification Methods Other Than $MTR_{asym}$(3.5 ppm)

There are several definitions and representations of the APTw effect. In addition to $MTR_{asym}$(3.5 ppm), $MTR_{asymnr}$, a normalization by the reference scan, $S_{sat}$ (–3.5 ppm) instead of $S_0$, is also used,[15,147] which leads to larger values. In an effort to more specifically assess the APT effect, several alternative postprocessing approaches have been proposed.[21,22,26–31] Most of these either use the Bloch–McConnell equations[21,22,26,27] or a sum of multiple Lorentzian shapes[28–30] to fit out background signals from DS and MTC and to study the remaining CEST-based signals, including APT and rNOE contributions. One of these data analysis approaches, EMR analysis (Eqs. [4, 5]),[21,22] tries to estimate background DS and MTC contributions based on extrapolating Z-spectral signals from outside the liquid-phase proton spectral range. Such background removal approaches seem more specific. For instance, they are more appropriate for studying ischemia to avoid partial canceling of two pH-dependent signals (APT and rNOE).[32] Outside the brain, the $MTR_{asym}$(3.5 ppm) approach suffers from artifacts from the upfield fat signal at –3.5 ppm. The background removal approaches also overcome this limitation, allowing possible imaging of prostate and breast cancers.

The original APTR analytical expression (Eq. [1]) under the weak saturation pulse approximation suggests that APTR depends on $T_{1w}$ linearly. This raises the concern of whether there is a need to normalize the $T_{1w}$ effect in APTR.[151,152] In this respect, it is important to assess how the APT effect in tissue under the used experimental condition depends on the water proton content and $T_{1w}$. A recent preclinical study at 4.7 T (a $B_1$ of 1.3 $\mu$T and a $t_{sat}$ of 4 sec)[76] demonstrated that even though both the water content and the $T_{1w}$ increased in the tumor compared with the normal brain tissue, the ratio $T_{1w}$/[water proton] remained nearly unchanged. This means that the effect of the increasing $T_{1w}$ on the measured APTw signals was mostly canceled out by the effect of the increasing water content in the tumor, as pointed out in the early APTw study.[10] Further, two recent numerical simulation studies[148,149] have clearly demonstrated that the $MTR_{asym}$ (3.5 ppm) signal increase with $T_{1w}$ at low $B_1$ (<1 $\mu$T), is roughly insensitive to $T_{1w}$ at intermediate $B_1$ (1.5–2.5 $\mu$T), and even slightly decreases with $T_{1w}$ at high $B_1$ (>3 $\mu$T), a complicated nonlinear relationship because of complicated differential equations. Those authors concluded that it may not be necessary to correct for the influence of $T_{1w}$ on APT- and NOE-based imaging of gliomas with the recommended saturation parameters ($B_1$ = 2 $\mu$T and $t_{sat}$ = 0.8–2 sec) for clinical 3 T MRI systems.

Recently, two alternative CEST metrics have been defined: $MTR_{Rex}$ (subtraction of inverse Z-spectra to correct for effects from DS and MTC)[150] and AREX (apparent exchange-dependent relaxation to remove the influence of the $T_{1w}$ contribution):[151,152]

$$MTR_{Rex} = 1/Z_{lab} - 1/Z_{ref} \quad (7)$$

$$AREX = MTR_{Rex}/T_{1w} \quad (8)$$

It is important to compare these terms with Eq. [1]. Dividing by $T_{1w}$ would make it independent of the transfer process and not a real CEST effect, but instead something like an exchange rate. More important, similar to $MTR_{asym}$(3.5 ppm), it is necessary to evaluate whether the $MTR_{Rex}$ signal in tissue depends on $T_{1w}$ linearly (an extreme

case achieved typically when there is no significant DS effect); otherwise, the AREX procedure will unavoidably introduce an extra $T_{1w}$ effect that changes the contrast for malignant tumors. Indeed, it has been reported in two recent studies[152,153] that the use of the AREX metric led to the disappearance of the tumor contrast ($AREX_{tumor} \approx AREX_{normal}$). However, this alternative contrast could also have some unique uses and certain advantages that have to be proven in more extensive patient studies.

### Confounding APTw MRI Signal Contributions: Artifactual and Real

Similar to other MRI sequences, APTw MRI is prone to some confounding signal contributions that may mislead and confuse its interpretation. These may have an origin in technical details or even the tissue components under investigation. From a technical point of view, $B_0$ inhomogeneity remains a critical issue in APTw imaging. The APTw signal is usually measured by the MTR asymmetry analysis between signal intensities of $\pm 3.5$ ppm with respect to the water frequency. As a consequence, the quality of APTw imaging greatly depends on the $B_0$ homogeneity over the volume imaged, which affects the water resonance position. At 3 T,[40] the $B_0$ field inhomogeneity typically is less than 20 Hz in the relevant brain regions, but could be more than 100 Hz near air–tissue interfaces (sinus, ear). This $B_0$ field inhomogeneity may cause artifacts in the APTw images, most of which can be removed inside the brain through the realignment of the water center frequency,[13] but some signal hyper- and hypointensities are sometimes found around the brain and in the skull (Figs. 4–6), which should not be confused with APTw effects.

APTw MRI signals are generated from water-exchangeable amide protons in mobile proteins and peptides in living tissues (ie, those in the cytoplasm, blood, or other body fluids). Thus, areas of large liquefactive necrosis, hemorrhage, or large vessels would typically demonstrate high APTw signals.[67,69,129] It is particularly important to note the inconsistency of APTw signal intensities of coagulative necrosis and liquefactive necrosis in the central regions of malignant gliomas, as identified by $T_2$w and FLAIR images.[23] Coagulative necrosis is characterized by the formation of a gelatinous (gel-like) substance in dead tissues. Liquefactive necrosis is characterized by the digestion of dead cells to form a viscous liquid mass, showing $T_2$w hyperintensity and substantially suppressed water signals on FLAIR images. It is expected that the proteins and peptides are prone to higher mobility in the microenvironment of liquefactive necrosis. The consequentially increased concentration of mobile proteins and peptides results in hyperintensity on the APTw image. On the other hand, coagulation necrosis largely restricts the mobility of proteins, leading to hypointensity on APTw images, which is similar to proteins in cooked egg white, showing almost zero APT effect.[154] Furthermore, the intratumoral vessels in low-grade gliomas always demonstrate hyperintensity on APTw images,[105] which highly resembles the hyperintensity from the malignant tumors. The scenario is similar to liver,[155] where the intrahepatic portal system and hepatic arteries always show hyperintensity on APTw images. In both cases, the mobile proteins in the blood generate strong endogenous APTw contrast as inherent problems. Fortunately, the areas of large liquefactive necrosis, hemorrhages, or large vessels are often evident on standard structural MRI sequences (such as $T_2$w, FLAIR, and $T_1$w). When reviewing APTw images, referring to routine structural MR images to identify "hyperintensity artifacts," such as liquefactive necrosis, cysts, hemorrhages, and vessels, is necessary for accurate interpretation. In addition, angiogenesis is often a hallmark of malignant tumors and the contribution of tumor vessels to APTw hyperintensity can be seen as natural.

## Conclusion

APTw MRI is a newly emerging molecular imaging technique that is based on mobile endogenous proteins and peptides in tissue and does not require exogenous contrast agent injection. The technique has been validated based on biopsies for clinical neuroimaging of brain tumors, and is showing promise for many other applications, including, but not limited to, imaging of ischemic and hemorrhagic stroke, AD, PD, MS, and TBI. Several challenging technical issues for clinical APTw imaging include scanner hardware constraints, complicated contrast mechanism with multiple contributions, and the possibility for $B_0$ inhomogeneity artifacts and lipid artifacts. In addition, differences in APTw pulse sequences and data processing strategies may complicate the reproducibility and comparison of results between hospitals. It is thus essential to understand the limitations of these techniques in order to accurately interpret the results. For the clinician to be able to use this methodology without needing to worry about such issues and to achieve consistency between different hospitals, it is important that the manufacturers implement an automated version of APTw MRI based on comparable parameters. For brain tumors, we recommend the use of $B_1 = 2\ \mu T$ and a total saturation time (with interpulse delays if needed) of 0.8–2 sec followed by $B_0$ correction and asymmetry analysis. For other diseases, acquisition and analysis approaches still need to be further optimized. It will be up to the MRI manufacturers to collaborate with the research and clinical communities to make sure that this will be done in a reliable and easy-to-use manner.

### Potential Conflict of Interest

J.Z. and P.C.M.v.Z. are coinventors on a patent for the APT MRI technology. This patent is owned and managed by Johns Hopkins University. P.C.M.v.Z. is a paid lecturer for Philips Medical Systems. This arrangement has been approved by

Johns Hopkins University in accordance with its Conflict of Interest policies.

## Acknowledgments

Contract grant sponsor: National Institutes of Health; Contract grant numbers: R01EB009731, R01EB015032, R01CA166171, R21CA227783, R01CA228188, UG3NS106937, and P41EB0 15909; Contract grant sponsor: Swedish Research Council; Contract grant numbers: 2015-04170 and 2017-00995; Contract grant sponsor: Swedish Cancer Society; Contract grant number: CAN 2015/251; Contract grant sponsor: Swedish Brain Foundation; Contract grant number: FO2017-0236. The supporting sources had no role in the study design or conduct, or in the decision to submit for publication.

## References

1. Weissleder R, Pittet MJ. Imaging in the era of molecular oncology. Nature 2008;452:580–589.
2. Forsen S, Hoffman RA. Study of moderately rapid chemical exchange reactions by means of nuclear magnetic double resonance. J Chem Phys 1963;39:2892–2901.
3. Ward KM, Aletras AH, Balaban RS. A new class of contrast agents for MRI based on proton chemical exchange dependent saturation transfer (CEST). J Magn Reson 2000;143:79–87.
4. Zhou J, van Zijl PC. Chemical exchange saturation transfer imaging and spectroscopy. Progr NMR Spectr 2006;48:109–136.
5. Sherry AD, Woods M. Chemical exchange saturation transfer contrast agents for magnetic resonance imaging. Annu Rev Biomed Eng 2008; 10:391–411.
6. Kogan F, Hariharan H, Reddy R. Chemical exchange saturation transfer (CEST) imaging: Description of technique and potential clinical applications. Curr Radiol Reports 2013;1:102–114.
7. Vinogradov E, Sherry AD, Lenkinski RE. CEST: From basic principles to applications, challenges and opportunities. J Magn Reson 2013;229: 155–172.
8. van Zijl PCM, Lam WW, Xu J, Knutsson L, Stanisz GJ. Magnetization transfer contrast and chemical exchange saturation transfer MRI. Features and analysis of the field-dependent saturation spectrum. NeuroImage 2018;168:222–241.
9. Jones KM, Pollard AC, Pagel MD. Clinical applications of chemical exchange saturation transfer (CEST) MRI. J Magn Reson Imaging 2018; 47:11–27.
10. Zhou J, Payen J, Wilson DA, Traystman RJ, van Zijl PCM. Using the amide proton signals of intracellular proteins and peptides to detect pH effects in MRI. Nat Med 2003;9:1085–1090.
11. Mori S, Eleff SM, Pilatus U, Mori N, van Zijl PCM. Proton NMR spectroscopy of solvent-saturable resonance: A new approach to study pH effects in situ. Magn Reson Med 1998;40:36–42.
12. van Zijl PCM, Zhou J, Mori N, Payen J, Mori S. Mechanism of magnetization transfer during on-resonance water saturation. A new approach to detect mobile proteins, peptides, and lipids. Magn Reson Med 2003; 49:440–449.
13. Zhou J, Blakeley JO, Hua J, et al. Practical data acquisition method for human brain tumor amide proton transfer (APT) imaging. Magn Reson Med 2008;60:842–849.
14. Zhou J, Wilson DA, Sun PZ, Klaus JA, van Zijl PCM. Quantitative description of proton exchange processes between water and endogenous and exogenous agents for WEX, CEST, and APT experiments. Magn Reson Med 2004;51:945–952.
15. Ling W, Regatte RR, Navon G, Jerschow A. Assessment of glycosaminoglycan concentration in vivo by chemical exchange-dependent saturation transfer (gagCEST). Proc Natl Acad Sci U S A 2008;105:2266–2270.
16. van Zijl PCM, Yadav NN. Chemical exchange saturation transfer (CEST): What is in a name and what isn't? Magn Reson Med 2011;65:927–948.
17. Jones CK, Huang A, Xu J, et al. Nuclear Overhauser enhancement (NOE) imaging in the human brain at 7T. NeuroImage 2013;77:114–124.
18. Lu J, Zhou J, Cai C, Cai S, Chen Z. Observation of true and pseudo NOE signals using CEST-MRI and CEST-MRS sequences with and without lipid suppression. Magn Reson Med 2015;73:1615–1622.
19. Hua J, Jones CK, Blakeley J, Smith SA, van Zijl PCM, Zhou J. Quantitative description of the asymmetry in magnetization transfer effects around the water resonance in the human brain. Magn Reson Med 2007;58:786–793.
20. Zhou J, Hong X, Zhao X, Gao J-H, Yuan J. APT-weighted and NOE-weighted image contrasts in glioma with different RF saturation powers based on magnetization transfer ratio asymmetry analyses. Magn Reson Med 2013;70:320–327.
21. Heo HY, Zhang Y, Jiang S, Lee DH, Zhou J. Quantitative assessment of amide proton transfer (APT) and nuclear overhauser enhancement (NOE) imaging with extrapolated semisolid magnetization transfer reference (EMR) signals: II. Comparison of three EMR models and application to human brain glioma at 3 Tesla. Magn Reson Med 2016;75: 1630–1639.
22. Heo HY, Zhang Y, Lee DH, Hong X, Zhou J. Quantitative assessment of amide proton transfer (APT) and nuclear overhauser enhancement (NOE) imaging with extrapolated semi-solid magnetization transfer reference (EMR) signals: Application to a rat glioma model at 4.7 Tesla. Magn Reson Med 2016;75:137–149.
23. Jiang S, Eberhart CG, Zhang Y, et al. Amide proton transfer-weighted MR image-guided stereotactic biopsy in patients with newly diagnosed gliomas. Eur J Cancer 2017;83:9–18.
24. Jiang S, Eberhart CG, Lim M, et al. Identifying recurrent malignant glioma after treatment using amide proton transfer-weighted MR imaging: A validation study with image-guided stereotactic biopsy. Clin Cancer Res 2018 doi: https://doi.org/10.1158/078-0432.CCR-18-1233 [Epub ahead of print].
25. U.S. Food and Drug Administration. Available at: https://www.accessdata.fda.gov/cdrh_docs/pdf17/K172920.pdf
26. Liu D, Zhou J, Xue R, Zuo Z, An J, Wang DJJ. Quantitative characterization of nuclear Overhauser enhancement and amide proton transfer effects in the human brain at 7 Tesla. Magn Reson Med 2013;70: 1070–1081.
27. Chappell MA, Donahue MJ, Tee YK, et al. Quantitative Bayesian model-based analysis of amide proton transfer MRI. Magn Reson Med 2013;70:556–567.
28. Zaiss M, Schmitt B, Bachert P. Quantitative separation of CEST effect from magnetization transfer and spillover effects by Lorentzian-line-fit analysis of z-spectra. J Magn Reson 2011;211:149–155.
29. Desmond KL, Moosvi F, Stanisz GJ. Mapping of amide, amine, and aliphatic peaks in the CEST spectra of murine xenografts at 7 T. Magn Reson Med 2014;71:1841–1853.
30. Cai K, Singh A, Poptani H, et al. CEST signal at 2ppm (CEST@2ppm) from Z-spectral fitting correlates with creatine distribution in brain tumor. NMR Biomed 2015;28:1–8.
31. Jin T, Wang P, Zong X, Kim S-G. MR imaging of the amide-proton transfer effect and the pH-insensitive nuclear Overhauser effect at 9.4 T. Magn Reson Med 2013;69:760–770.
32. Heo HY, Zhang Y, Burton TM, et al. Improving the detection sensitivity of pH-weighted amide proton transfer MRI in acute stroke patients using extrapolated semisolid magnetization transfer reference signals. Magn Reson Med 2017;78:871–880.
33. Scheidegger R, Vinogradov E, Alsop DC. Amide proton transfer imaging with improved robustness to magnetic field inhomogeneity and magnetization transfer asymmetry using saturation with frequency alternating RF irradiation. Magn Reson Med 2011;66:1275–1285.

34. Lee JS, Regatte RR, Jerschow A. Isolating chemical exchange saturation transfer contrast from magnetization transfer asymmetry under two-frequency rf irradiation. J Magn Reson 2012;215:56–63.

35. Lee JS, Xia D, Ge Y, Jerschow A, Regatte RR. Concurrent saturation transfer contrast in in vivo brain by a uniform magnetization transfer MRI. NeuroImage 2014;95:22–28.

36. Zu Z, Janve VA, Xu J, Does MD, Gore JC, Gochberg DF. A new method for detecting exchanging amide protons using chemical exchange rotation transfer. Magn Reson Med 2013;69:637–647.

37. Xu J, Yadav NN, Bar-Shir A, et al. Variable delay multi-pulse train for fast chemical exchange saturation transfer and relayed-nuclear overhauser enhancement MRI. Magn Reson Med 2014;71:1798–1812.

38. Zhou Z, Han P, Zhou B, et al. Chemical exchange saturation transfer fingerprinting for exchange rate quantification. Magn Reson Med 2018;80: 1352–1363.

39. Cohen O, Huang S, McMahon MT, Rosen MS, Farrar CT. Rapid and quantitative chemical exchange saturation transfer (CEST) imaging with magnetic resonance fingerprinting (MRF). Magn Reson Med 2018 doi: https://doi.org/10.1002/mrm.27221 [Epub ahead of print].

40. Zhu H, Jones CK, van Zijl PCM, Barker PB, Zhou J. Fast 3D chemical exchange saturation transfer (CEST) imaging of the human brain. Magn Reson Med 2010;64:638–644.

41. Dula AN, Arlinghaus LR, Dortch RD, et al. Amide proton transfer imaging of the breast at 3 T: Establishing reproducibility and possible feasibility assessing chemotherapy response. Magn Reson Med 2013;70:216–224.

42. Dixon WT, Hancu I, Ratnakar SJ, Sherry AD, Lenkinski RE, Alsop DC. A multislice gradient echo pulse sequence for CEST imaging. Magn Reson Med 2009;63:253–256.

43. Scheidegger R, Wong ET, Alsop DC. Contributors to contrast between glioma and brain tissue in chemical exchange saturation transfer sensitive imaging at 3 Tesla. NeuroImage 2014;99:256–268.

44. Sun PZ, Benner T, Kumar A, Sorensen AG. Investigation of optimizing and translating pH-sensitive pulsed-chemical exchange saturation transfer (CEST) imaging to a 3T clinical scanner. Magn Reson Med 2008;60:834–841.

45. Schmitt B, Zaiß M, Zhou J, Bachert P. Optimization of pulse train presaturation for CEST imaging in clinical scanners. Magn Reson Med 2011; 65:1620–1629.

46. Tee YK, Harston GW, Blockley N, et al. Comparing different analysis methods for quantifying the MRI amide proton transfer (APT) effect in hyperacute stroke patients. NMR Biomed 2014;27:1019–1029.

47. Keupp J, Baltes C, Harvey PR, van den Brink J. Parallel RF transmission based MRI technique for highly sensitive detection of amide proton transfer in the human brain. In: Proc 19th Annual Meeting ISMRM, Montreal; 2011. p 710.

48. Togao O, Hiwatashi A, Keupp J, et al. Amide proton transfer imaging of diffuse gliomas: Effect of saturation pulse length in parallel transmission-based technique. PLoS One 2016;11:e0155925.

49. Jones CK, Polders D, Hua J, et al. In vivo 3D whole-brain pulsed steady state chemical exchange saturation transfer at 7T. Magn Reson Med 2012;67:1579–1589.

50. Zhao X, Wen Z, Huang F, et al. Saturation power dependence of amide proton transfer image contrasts in human brain tumors and strokes at 3 T. Magn Reson Med 2011;66:1033–1041.

51. Zhao X, Wen Z, Zhang G, et al. Three-dimensional turbo-spin-echo amide proton transfer MR imaging at 3-Tesla and its application to high-grade human brain tumors. Mol Imaging Biol 2013;15:114–122.

52. Varma G, Lenkinski R, Vinogradov E. Keyhole chemical exchange saturation transfer. Magn Reson Med 2012;68:1228–1233.

53. Zhang Y, Heo HY, Jiang S, Lee DH, Bottomley PA, Zhou J. Highly accelerated chemical exchange saturation transfer (CEST) measurements with linear algebraic modeling. Magn Reson Med 2016;76:136–144.

54. Zhang Y, Heo HY, Lee DH, et al. Chemical exchange saturation transfer (CEST) imaging with fast variably-accelerated sensitivity encoding (vSENSE). Magn Reson Med 2017;77:2225–2238.

55. Heo HY, Zhang Y, Lee DH, Jiang S, Zhao X, Zhou J. Accelerating chemical exchange saturation transfer (CEST) MRI by combining compressed sensing and sensitivity encoding techniques. Magn Reson Med 2017;77:779–786.

56. Zaiss M, Ehses P, Scheffler K. Snapshot-CEST: Optimizing spiral-centric-reordered gradient echo acquisition for fast and robust 3D CEST MRI at 9.4 T. NMR Biomed 2018;31:e3879.

57. Kim M, Gillen J, Landman BA, Zhou J, van Zijl PCM. Water saturation shift referencing (WASSR) for chemical exchange saturation transfer (CEST) experiments. Magn Reson Med 2009;61:1441–1450.

58. Liu G, Gilad AA, Bulte JW, van Zijl PC, McMahon MT. High-throughput screening of chemical exchange saturation transfer MR contrast agents. Contrast Media Mol Imaging 2010;5:162–170.

59. Wei W, Jia G, Flanigan D, Zhou J, Knopp MV. Chemical exchange saturation transfer MR imaging of articular cartilage glycosaminoglycans at 3 T: Accuracy of $B_0$ field Inhomogeneity corrections with gradient echo method. Magn Reson Imaging 2014;32:41–47.

60. Keupp J, Eggers H. CEST-Dixon MRI for sensitive and accurate measurement of amide proton transfer in humans at 3T. In: Proc 18th Annual Meeting ISMRM, Stockholm; 2010. p 338.

61. Togao O, Keupp J, Hiwatashi A, et al. Amide proton transfer imaging of brain tumors using a self-corrected 3D fast spin-echo Dixon method: Comparison with separate B0 correction. Magn Reson Med 2017;77:2272–2279.

62. Schuenke P, Windschuh J, Roeloffs V, Ladd ME, Bachert P, Zaiss M. Simultaneous mapping of water shift and B1 (WASABI)-Application to field-Inhomogeneity correction of CEST MRI data. Magn Reson Med 2017;77:571–580.

63. Eidel O, Burth S, Neumann JO, et al. Tumor infiltration in enhancing and non-enhancing parts of glioblastoma: A correlation with histopathology. PLoS One 2017;12:e0169292.

64. Brindle KM, Izquierdo-Garcia JL, Lewis DY, Mair RJ, Wright AJ. Brain tumor imaging. J Clin Oncol 2017;35:2432–2438.

65. Zhou J, Lal B, Wilson DA, Laterra J, van Zijl PCM. Amide proton transfer (APT) contrast for imaging of brain tumors. Magn Reson Med 2003;50: 1120–1126.

66. Salhotra A, Lal B, Laterra J, Sun PZ, van Zijl PCM, Zhou J. Amide proton transfer imaging of 9L gliosarcoma and human glioblastoma xenografts. NMR Biomed 2008;21:489–497.

67. Grossman R, Tyler B, Brem H, et al. Growth properties of SF188/V+ human glioma in rats in vivo observed by magnetic resonance imaging. J Neuro Oncol 2012;110:315–323.

68. Jones CK, Schlosser MJ, van Zijl PC, Pomper MG, Golay X, Zhou J. Amide proton transfer imaging of human brain tumors at 3T. Magn Reson Med 2006;56:585–592.

69. Wen Z, Hu S, Huang F, et al. MR imaging of high-grade brain tumors using endogenous protein and peptide-based contrast. NeuroImage 2010;51:616–622.

70. Jiang S, Yu H, Wang X, et al. Molecular MRI differentiation between primary central nervous system lymphomas and high-grade gliomas using endogenous protein-based amide proton transfer MR imaging at 3 Tesla. Eur Radiol 2016;26:64–71.

71. Yu H, Lou H, Zou T, et al. Applying protein-based amide proton transfer MR imaging to distinguish solitary brain metastases from glioblastoma. Eur Radiol 2017;27:4516–4524.

72. Sakata A, Fushimi Y, Okada T, et al. Diagnostic performance between contrast enhancement, proton MR spectroscopy, and amide proton transfer imaging in patients with brain tumors. J Magn Reson Imaging 2017;46:732–739.

73. Joo B, Han K, Choi YS, et al. Amide proton transfer imaging for differentiation of benign and atypical meningiomas. Eur Radiol 2018;28: 331–339.

74. Sun H, Xin J, Zhou J, Lu Z, Guo Q. Applying amide proton transfer MR imaging to hybrid brain PET/MR: Concordance with gadolinium enhancement and added value to [(18)F]FDG PET. Mol Imaging Biol 2018;20:473–481.

75. Lindeman LR, Randtke EA, High RA, Jones KM, Howison CM, Pagel MD. A comparison of exogenous and endogenous CEST MRI methods for evaluating in vivo pH. Magn Reson Med 2018;79:2766–2772.

76. Lee DH, Heo HY, Zhang K, et al. Quantitative assessment of the effects of water proton concentration and water T1 changes on amide proton transfer (APT) and nuclear overhauser enhancement (NOE) MRI: The origin of the APT imaging signal in brain tumor. Magn Reson Med 2017; 77:855–863.

77. Hobbs SK, Shi G, Homer R, Harsh G, Altlas SW, Bednarski MD. Magnetic resonance imaging-guided proteomics of human glioblastoma multiforme. J Magn Reson Imag 2003;18:530–536.

78. Yan K, Fu Z, Yang C, et al. Assessing amide proton transfer (APT) MRI contrast origins in 9L gliosarcoma in the rat brain using proteomic analysis. Mol Imaging Biol 2015;17:479–487.

79. Howe FA, Barton SJ, Cudlip SA, et al. Metabolic profiles of human brain tumors using quantitative in vivo $^{1}$H magnetic resonance spectroscopy. Magn Reson Med 2003;49:223–232.

80. Griffiths JR. Are cancer cells acidic? Br J Cancer 1991;64:425–427.

81. Zhou J, Zhu H, Lim M, et al. Three-dimensional amide proton transfer MR imaging of gliomas: Initial experience and comparison with gadolinium enhancement. J Magn Reson Imaging 2013;38:1119–1128.

82. Togao O, Yoshiura T, Keupp J, et al. Amide proton transfer imaging of adult diffuse gliomas: Correlation with histopathological grades. Neuro Oncol 2014;16:441–448.

83. Sakata A, Okada T, Yamamoto A, et al. Grading glial tumors with amide proton transfer MR imaging: Different analytical approaches. J Neuro Oncol 2015;122:339–348.

84. Togao O, Hiwatashi A, Yamashita K, et al. Grading diffuse gliomas without intense contrast enhancement by amide proton transfer MR imaging: Comparisons with diffusion- and perfusion-weighted imaging. Eur Radiol 2017;27:578–588.

85. Su C, Liu C, Zhao L, et al. Amide proton transfer imaging allows detection of glioma grades and tumor proliferation: Comparison with Ki-67 expression and proton MR spectroscopy imaging. AJNR Am J Neuroradiol 2017;38:1702–1709.

86. Choi YS, Ahn SS, Lee SK, et al. Amide proton transfer imaging to discriminate between low- and high-grade gliomas: Added value to apparent diffusion coefficient and relative cerebral blood volume. Eur Radiol 2017;27:3181–3189.

87. Zou T, Yu H, Jiang C, et al. Differentiating the histologic grades of gliomas preoperatively using amide proton transfer-weighted (APTW) and intravoxel incoherent motion MRI. NMR Biomed 2018;31:e3850.

88. Zhang J, Zhu W, Tain R, Zhou XJ, Cai K. Improved differentiation of low-grade and high-grade gliomas and detection of tumor proliferation using APT contrast fitted from Z-spectrum. Mol Imaging Biol 2018;20:623–631.

89. Scott JN, Brasher PM, Sevick RJ, Rewcastle NB, Forsyth PA. How often are nonenhancing supratentorial gliomas malignant? A population study. Neurology 2002;59:947–949.

90. Knopp EA, Cha S, Johnson G, et al. Glial neoplasms: Dynamic contrast-enhanced T2*-weighted MR imaging. Radiology 1999;211:791–798.

91. Wen PY, Macdonald DR, Reardon DA, et al. Updated response assessment criteria for high-grade gliomas: Response assessment in neuro-oncology working group. J Clin Oncol 2010;28:1963–1972.

92. Zhou J, Tryggestad E, Wen Z, et al. Differentiation between glioma and radiation necrosis using molecular magnetic resonance imaging of endogenous proteins and peptides. Nat Med 2011;17:130–134.

93. Wang SL, Tryggestad E, Zhou TT, et al. Assessment of MRI parameters as imaging biomarkers for radiation necrosis in the rat brain. Int J Radiat Oncol Biol Phys 2012;83:E431–E436.

94. Hong X, Liu L, Wang M, et al. Quantitative multiparametric MRI assessment of glioma response to radiotherapy in a rat model. Neuro Oncol 2014;16:856–867.

95. Sagiyama K, Mashimo T, Togao O, et al. In vivo chemical exchange saturation transfer imaging allows early detection of a therapeutic response in glioblastoma. Proc Natl Acad Sci U S A 2014;111:4542–4527.

96. Hectors S, Jacobs I, Strijkers GJ, Nicolay K. Amide proton transfer imaging of high intensity focused ultrasound-treated tumor tissue. Magn Reson Med 2014;72:1113–1122.

97. Zhou J. Response assessment of human brain tumors using amide proton transfer imaging at 3T. Contrast Media Mol Imaging 2013;8:308–309.

98. Ma B, Blakeley JO, Hong X, et al. Applying amide proton transfer-weighted MRI to distinguish pseudoprogression from true progression in malignant gliomas. J Magn Reson Imaging 2016;44:456–462.

99. Park JE, Kim HS, Park KJ, Kim SJ, Kim JH, Smith SA. Pre- and posttreatment glioma: Comparison of amide proton transfer imaging with MR spectroscopy for biomarkers of tumor proliferation. Radiology 2016; 278:514–523.

100. Park KJ, Kim HS, Park JE, Shim WH, Kim SJ, Smith SA. Added value of amide proton transfer imaging to conventional and perfusion MR imaging for evaluating the treatment response of newly diagnosed glioblastoma. Eur Radiol 2016;26:4390–4403.

101. Desmond KL, Mehrabian H, Chavez S, et al. Chemical exchange saturation transfer for predicting response to stereotactic radiosurgery in human brain metastasis. Magn Reson Med 2017;78:1110–1120.

102. Louis DN, Perry A, Reifenberger G, et al. The 2016 World Health Organization classification of tumors of the central nervous system: A summary. Acta Neuropathol 2016;131:803–820.

103. Choi C, Ganji SK, DeBerardinis RJ, et al. 2-Hydroxyglutarate detection by magnetic resonance spectroscopy in subjects with IDH-mutated gliomas. Nat Med 2012;18:624–629.

104. de la Fuente MI, Young RJ, Rubel J, et al. Integration of 2-hydroxyglutarate-proton magnetic resonance spectroscopy into clinical practice for disease monitoring in isocitrate dehydrogenase-mutant glioma. Neuro Oncol 2016;18:283–290.

105. Jiang S, Zou T, Eberhart CG, et al. Predicting IDH mutation status in grade II gliomas using amide proton transfer-weighted (APTw) MRI. Magn Reson Med 2017;78:1100–1109.

106. Jiang S, Rui Q, Wang Y, et al. Discriminating MGMT promoter methylation status in patients with glioblastoma employing amide proton transfer-weighted MRI metrics. Eur Radiol 2018;28:2115–2123.

107. Doll S, Urisman A, Oses-Prieto JA, Arnott D, Burlingame AL. Quantitative proteomics reveals fundamental regulatory differences in oncogenic HRAS and isocitrate dehydrogenase (IDH1) driven astrocytoma. Mol Cell Proteomics 2017;16:39–56.

108. Paech D, Windschuh J, Oberhollenzer J, et al. Assessing the predictability of IDH mutation and MGMT methylation status in glioma patients using relaxation-compensated multi-pool CEST MRI at 7.0 Tesla. Neuro Oncol 2018 doi: https://doi.org/10.1093/neuonc/noy073 [Epub ahead of print].

109. Su L, Gao P, Lin S, et al. Predicting O6-methylguanine-DNA methyltransferase protein expression in primary low- and high-grade gliomas using certain qualitative characteristics of amide proton transfer-weighted magnetic resonance imaging. World Neurosurg 2018;116: E814–E823.

110. Astrup J. Thresholds of cerebral ischemia. In: Schmiedek P, ed. *Microsurgery for stroke*. Berlin: Springer; 1976. p 16–21.

111. Warach S, Dashe JF, Edelman RR. Clinical outcome in ischemic stroke predicted by early diffusion-weighted and perfusion magnetic resonance imaging: A preliminary analysis. J Cereb Blood Flow Metab 1996;16:53–59.

112. Donahue MJ, Achten E, Cogswell PM, et al. Consensus statement on current and emerging methods for the diagnosis and evaluation of cerebrovascular disease. J Cereb Blood Flow Metab 2018;38: 1391–1417.

113. Leigh R, Knutsson L, Zhou J, van Zijl PC. Imaging the physiological evolution of the ischemic penumbra in acute ischemic stroke. J Cereb Blood Flow Metab 2018;38:1500–1516.

114. Zhou JY, van Zijl PCM. Defining an acidosis-based ischemic penumbra from pH-weighted MRI. Transl Stroke Res 2012;3:76–83.

115. Sun PZ, Zhou J, Sun W, Huang J, van Zijl PCM. Detection of the ischemic penumbra using pH-weighted MRI. J Cereb Blood Flow Metab 2007;27:1129–1136.

116. Jokivarsi KT, Grohn HI, Grohn OH, Kauppinen RA. Proton transfer ratio, lactate, and intracellular pH in acute cerebral ischemia. Magn Reson Med 2007;57:647–653.

117. Sun PZ, Cheung JS, Wang E, Berner T, Sorensen AG. Fast multislice pH-weighted chemical exchange saturation transfer (CEST) MRI with unevenly segmented RF irradiation. Magn Reson Med 2011;65: 588–594.

118. Sun PZ, Wang EF, Cheung JS. Imaging acute ischemic tissue acidosis with pH-sensitive endogenous amide proton transfer (APT) MRI-Correction of tissue relaxation and concomitant RF irradiation effects toward mapping quantitative cerebral tissue pH. NeuroImage 2012; 60:1–6.

119. Jin T, Wang P, Zong XP, Kim SG. Magnetic resonance imaging of the Amine-Proton EXchange (APEX) dependent contrast. NeuroImage 2012;59:1218–1227.

120. Zong XP, Wang P, Kim SG, Jin T. Sensitivity and source of amine-proton exchange and amide-proton transfer magnetic resonance imaging in cerebral ischemia. Magn Reson Med 2014;71:118–132.

121. McVicar N, Li AX, Goncalves DF, et al. Quantitative tissue pH measurement during cerebral ischemia using amine and amide concentration-independent detection (AACID) with MRI. J Cereb Blood Flow Metab 2014;34:690–698.

122. Guo YK, Zhou IY, Chan ST, et al. pH-sensitive MRI demarcates graded tissue acidification during acute stroke — pH specificity enhancement with magnetization transfer and relaxation-normalized amide proton transfer (APT) MRI. NeuroImage 2016;141:242–249.

123. Jin T, Wang P, Hitchens TK, Kim SG. Enhancing sensitivity of pH-weighted MRI with combination of amide and guanidyl CEST. NeuroImage 2017;157:341–350.

124. Tietze A, Blicher J, Mikkelsen IK, et al. Assessment of ischemic penumbra in patients with hyperacute stroke using amide proton transfer (APT) chemical exchange saturation transfer (CEST) MRI. NMR Biomed 2014; 27:163–174.

125. Harston GW, Tee YK, Blockley N, et al. Identifying the ischaemic penumbra using pH-weighted magnetic resonance imaging. Brain 2015; 138:36–42.

126. Song G, Li C, Luo X, et al. Evolution of cerebral ischemia assessed by amide proton transfer-weighted MRI. Front Neurol 2017;8:67.

127. Wang M, Hong X, Chang CF, et al. Simultaneous detection and separation of hyperacute intracerebral hemorrhage and cerebral ischemia using amide proton transfer MRI. Magn Reson Med 2015;74:42–50.

128. Zheng SK, van der Bom IMJ, Zu ZL, Lin GX, Zhao YS, Gounis MJ. Chemical exchange saturation transfer effect in blood. Magn Reson Med 2014;71:1082–1092.

129. Jeong HK, Han K, Zhou J, et al. Characterizing amide proton transfer imaging in haemorrhage brain lesions using 3T MRI. Eur Radiol 2017; 27:1577–1484.

130. Ma X, Bai Y, Lin Y, et al. Amide proton transfer magnetic resonance imaging in detecting intracranial hemorrhage at different stages: A comparative study with susceptibility weighted imaging. Sci Rep 2017; 7:45696.

131. Wang R, Li SY, Chen M, et al. Amide proton transfer magnetic resonance imaging of Alzheimer's disease at 3.0 Tesla: A preliminary study. Chin Med J 2015;128:615–619.

132. Dauer W, Przedborski S. Parkinson's disease: Mechanisms and models. Neuron 2003;39:889–909.

133. Li C, Peng S, Wang R, et al. Chemical exchange saturation transfer MR imaging of Parkinson's disease at 3 Tesla. Eur Radiol 2014;24: 2631–2639.

134. Li CM, Wang R, Chen HB, et al. Chemical exchange saturation transfer MR imaging is superior to diffusion-tensor imaging in the diagnosis and severity evaluation of Parkinson's disease: A study on substantia nigra and striatum. Front Aging Neurosci 2015;7:198.

135. Li CM, Chen M, Zhao XN, et al. Chemical exchange saturation transfer MRI signal loss of the substantia nigra as an imaging biomarker to evaluate the diagnosis and serverity of Parkinson's disease. Front Neurosci 2017;11:489.

136. Hodaie M, Neimat JS, Lozano AM. The dopaminergic nigrostriatal system and Parkinson's disease: Molecular events in development, disease, and cell death, and new therapeutic strategies. Neurosurgery 2007;60:17–28.

137. Tong JC, Wong H, Guttman M, et al. Brain alpha-synuclein accumulation in multiple system atrophy, Parkinson's disease and progressive supranuclear palsy: A comparative investigation. Brain 2010;133: 172–188.

138. Reich DS, Lucchinetti CF, Calabresi PA. Multiple sclerosis. N Engl J Med 2018;378:169–180.

139. Dula AN, Asche EM, Landman BA, et al. Development of chemical exchange saturation transfer at 7T. Magn Reson Med 2011;66:831–838.

140. By S, Barry RL, Smith AK, et al. Amide proton transfer CEST of the cervical spinal cord in multiple sclerosis patients at 3T. Magn Reson Med 2018;79:806–814.

141. Zhang H, Wang W, Jiang S, et al. Amide proton transfer-weighted MRI detection of traumatic brain injury in rats. J Cereb Blood Flow Metab 2017;37:3422–3432.

142. Wang W, Zhang H, Lee DH, et al. Using functional and molecular MRI techniques to detect neuroinflammation and neuroprotection after traumatic brain injury. Brain Behav Immun 2017;64:344–353.

143. Mehrabian H, Desmond KL, Soliman H, Sahgal A, Stanisz GJ. Differentiation between radiation necrosis and tumor progression using chemical exchange saturation transfer. Clin Cancer Res 2017;23:3667–3675.

144. The 7th International Workshop on Chemical Exchange Saturation Transfer (CEST) imaging. Available at: http://cest2018.medmeeting.org

145. Haris M, Nanga RPR, Singh A, et al. Exchange rates of creatine kinase metabolites: Feasibility of imaging creatine by chemical exchange saturation transfer MRI. NMR Biomed 2012;25:1305–1309.

146. Woessner DE, Zhang S, Merritt ME, Sherry AD. Numerical solution of the Bloch equations provides insights into the optimum design of PARACEST agents for MRI. Magn Reson Med 2005;53:790–799.

147. Cai KJ, Haris M, Singh A, et al. Magnetic resonance imaging of glutamate. Nat Med 2012;18:302–306.

148. Heo HY, Lee DH, Zhang Y, et al. Insight into the quantitative metrics of chemical exchange saturation transfer (CEST) imaging. Magn Reson Med 2017;77:1853–1865.

149. Zu ZL. Towards the complex dependence of MTRasym on T-1w in amide proton transfer (APT) imaging. NMR Biomed 2018;31:e3934.

150. Zaiss M, Bachert P. Chemical exchange saturation transfer (CEST) and MR Z-spectroscopy in vivo: A review of theoretical approaches and methods. Phys Med Biol 2013;58:R221–2R69.

151. Zaiss M, Xu J, Goerke S, et al. Inverse Z-spectrum analysis for spillover-, MT-, and T1-corrected steady-state pulsed CEST-MRI — application to pH-weighted MRI of acute stroke. NMR Biomed 2014;27:240–252.

152. Xu J, Zaiss M, Zu Z, et al. On the origins of chemical exchange saturation transfer (CEST) contrast in tumors at 9.4 T. NMR Biomed 2014;27: 406–416.

153. Zaiss M, Windschuh J, Paech D, et al. Relaxation-compensated CEST-MRI of the human brain at 7 T: Unbiased insight into NOE and amide signal changes in human glioblastoma. NeuroImage 2015;112:180–188.

154. Zhou JY, Yan K, Zhu H. A simple model for understanding the origin of the amide proton transfer MRI signal in tissue. Appl Magn Reson 2012; 42:393–402.

155. Chen SZ, Yuan J, Deng M, Wei J, Zhou J, Wang YX. Chemical exchange saturation transfer (CEST) MR technique for in-vivo liver imaging at 3.0 Tesla. Eur Radiol 2016;26:1792–1800.